NONSTATISTICAL INVERSION DYNAMICS OF T-SHAPED Ar_3

NONSTATISTICAL INVERSION DYNAMICS OF T-SHAPED Ar_3

By

SHASHI JAIN, Ph.D.

A Thesis

Submitted to the School of Graduate Studies

in Partial Fulfillment of the Requirements

for the Degree

Master of Science

McMaster University

MASTER OF SCIENCE (1991) McMaster University

Hamilton, Ontario

TITLE: Nonstatistical Inversion Dynamics of T-shaped Ar_3.

AUTHOR: Shashi Jain, Ph. D. (Indian Institute of Technology, Kanpur, India)

SUPERVISOR: Dr. Randall S. Dumont

NUMBER OF PAGES: x , 60

Abstract:

The objective of this research project was to study applications of statistical unimolecular reaction theories to a simple model chemical process. Such studies are needed to test the existing theories and provide direction for their further development. T-shaped Ar_3 , a simple chaotic two degree of freedom system, is an excellent candidate for such study, since statistical behavior is generally associated with chaotic dynamics.

Chemical kinetics predicts fully statistical decay curves of microcanonical population associated with one of the two equivalent arrangements of T-shaped Ar_3. However numerical computations, presented here, reveal nonstatistical characteristics of microcanonical T-shaped Ar_3 inversion at energies associated with strongly chaotic dynamics. Nonstatisticality is most pronounced at higher energies where internal relaxation time scales are comparable to the inversion time. At such energies, population decay curves exhibit damped oscillations about the equilibrium population. At energies just above the inversion threshold, where inversion is very slow, near statistical nonoscillatory behavior is observed. The "absorbing barrier method" of J.E. Straub and B.J. Berne [J. Chem. Phys. 83, 1138 (1985)] is shown to provide a reasonable model for observed population decays. Characteristics of corresponding gap distributions are described in terms of an adapted "delayed lifetime gap model". Analysis of the model which combines the absorbing barrier method and the adapted delayed lifetime gap model provides insight into the observation of both oscillatory and

nonoscillatory population decays. Specifically, the analysis describes the observations in terms of an "underdamped" or "overdamped" harmonic oscillator, respectively.

ACKNOWLEDGEMENTS

I would like to express my sincere gratitude to Dr. R. S. Dumont, my research supervisor, for his valuable guidance and endless encouragement in the course of this research project. His patience and consideration made the hard times much easier to go through. I am also grateful to Dr. Siegfried Bleher for valuable discussions, suggestions and comments during the course of this work.

I owe special thanks to my family members who have always been supportive and provided encouragement all the time.

Finally , the financial assistance of the Chemistry Department is gratefully acknowledged.

TABLE OF CONTENTS

LIST OF TABLES

LIST OF FIGURES

Chapter 1

Introduction

Chapter 1

Introduction

Traditional statistical theories of chemical reactions, such as Rice-Ramsberger-Kassel-Marcus (RRKM) and transition-state theories[1], have been remarkably successful as a practical means of calculating rate constants directly in terms of reacting species potential-energy characteristics[2]. This has been an invaluable aid to kineticists who do not wish to do large-scale dynamics computations. However, these theories are not without limitations[3]. Problems result from the breakdown of their implicit assumptions about the underlying dynamics. The RRKM rate constant depends on an equilibrium microcanonical average and thus does not depend on molecular dynamics. This breakdown has prompted a number of studies whose goal is to devise improved statistical theories which account for important dynamical effects. For example, recent investigations[4] have identified "bottlenecks" in phase space as a source of nonstatisticality. These bottlenecks are generalized transition states which determine the relevant unimolecular processes and their associated time scales. In this approach, rate constants associated with the relevant processes are estimated as ratios of flux to phase-space volume, just as in traditional calculations[2,5a].

Another method of improving statistical theories of unimolecular decomposition is based on the partitioning of phase space into "direct" and "strong collision" components, with only the latter component treated statistically[6]. In this method, one

keeps track of the "divergence" of trajectories initially adjacent on the transition state at the entrance to the metastable reactant complex region. If the divergence exceeds a predetermined threshold before the trajectories exit into product channels, then the trajectories are part of the strong collision component and are therefore taken to be subject to statistical treatment. In this way, this "divergence" method avoids the detailed examination of phase space necessary in a bottleneck analysis[7].

The chemical kinetics treatment of a unimolecular reaction is straightforward . Chemical equations for the reaction are established and directly translated into a set of linear kinetics equations. The latter are solved by diagonalizing the matrix of rate constants and the vector of populations at time t , C(t) , is determined uniquely in terms of its initial value, C(0) . An exact dynamical treatment of unimolecular reaction is not so straightforward. While it is posssible, in principle, to numerically solve the classical equations of motion associated with the reaction, such a solution would give the phase space properties which in turn have to be related to chemically interesting properties such as populations . Since kinetics represents some sort of approximation to an exact dynamics treatment, the traditional statistical approach is to take kinetics for granted and use dynamics considerations to evaluate the required rate constants. Kinetics is valid only if the dynamics is both ergodic and mixing. Recent articles[5] have used these characteristics of dynamics to develop generalized statistical theories of unimolecular reactions. These theories provide refined estimates of rate constants and go beyond simple kinetics to account for certain "nonstatistical" dynamical effects.

Recent progress[5], made on the foundations of statistical theories of unimolecular reactions[2], demands dynamical studies of simple model chemical processes. Such studies are needed to test the theories and provide direction for their further development. T-shaped Ar_3 , a simple chaotic[8] two degree of freedom system,

is an excellent candidate for such a study, since statistical behavior is generally associated with chaotic dynamics. However, numerical computations, presented here , indicate that this process is not statistical[9], except at energies very close to the inversion threshold. Microcanonical population decay curves, associated with one of the two equivalent arrangements of T-shaped Ar_3 , are generally not simple exponential. They are therefore, not consistent with a simple kinetics treatment, characteristic of full statisticality[5c,d].

While T-shaped Ar_3 population decay curves are not simple exponential, they are well modeled by the "absorbing barrier method", or ABM, of Straub and Berne[10] (see Chapter 3). This suggests that the process dynamics satisfy the assumption of chaos employed by the ABM. To understand how the statistical ABM is able to model the observed process nonstatisticality, we consider the nature of the ABM approximation. Specifically, the ABM assumes independence of successive "gap times", and reduces the inversion process to two independent virtual unimolecular decays, each characterized by a "gap distribution" which must be computed explicitly. It is the T-shaped Ar_3 gap distributions which manifest the observed nonstatisticality. The principle goal of the present work is to rationalize and model these gap distributions, and thereby characterize the nonstatisticality of the inversion population decays.

The delayed life-time gap model[5a], or DLGM , is a statistical theory of unimolecular decay which goes beyond the fully statistical simple exponential gap distribution. It generalizes simple unimolecular decay kinetics by allowing for "direct trajectories", and by accounting for finitely rapid "internal relaxation". It is based on observations of ideally chaotic model dynamical systems[11], and has been successfully applied to the decay of "open stadium billiard" systems.[5b,c] However, we see in

Chapter 4 , that a simple application of the DLGM cannot describe T-shaped Ar_3 inversion gap distributions. It is necessary to adapt the DLGM via introduction of an additional delay time. The additional delay is distinct from the usual delay/relaxation time inherent in previous formulations of the DLGM.

In combination with the ABM, the adapted DLGM provides a generalized statistical model of the T-shaped Ar_3 inversion process. The model incorporates, via the adapted DLGM, two delay times which characterize internal relaxation processes. Statisticality of the inversion dynamics occurs only when the inversion time scale is much longer than the relaxation times. Observed nonstatistical behavior results when this condition is not met, and the relaxation time scales are manifest in inversion population decay curves.

We begin, in Chapter 2, with a review of the classical dynamics theory of isomerization. There we define survival probability, reactive flux and the flux-flux correlation, emphasisizing both their physical significance and their importance in numerical computations. Chapter 3 deals with the absorbing boundary method and its basis in terms of the delayed life-time gap model. In Chapter 4, the DLGM is adapted to model the T-shaped Ar_3 inversion process. There, model survival probabilities are obtained by combining the adapted delayed life time gap model and the absorbing boundary method and are shown to reproduce the characteristics of the observed survival probabilities. An analysis of the generalized statistical model provides a damped harmonic oscillator analog to the inversion process. When the inversion time scale is long, the harmonic oscillator is in its "overdamped" regime where it exhibits no oscillations. A shorter inversion time scale corresponds to an "underdamped" harmonic oscillator which exhibits damped oscillations.

Chapter 2

Inversion Dynamics of T-shaped Ar_3

Chapter 2

Inversion Dynamics of T-shaped Ar_3

In the following classical mechanics treatment of Ar_3, argon atoms are restricted to a T-shaped configuration which is conserved under time evolution due to symmetry. It determines a two degree of freedom Hamiltonian system which admits a simple intramolecular "inversion" process. Inversion corresponds to passage of the axial Ar atom between the other two atoms (see Fig. 1). Further, it is assumed that process takes place in strict isolation. Modeling the potential with two body interactions only, and using the two body potential of Aziz and Slaman[12], the inversion threshold, E_{thres}, is given by the Ar_3 saddle point energy of 140.38 K [13a]. Figure 2 shows a contour plot of the model potential energy surface and a typical inversion trajectory.

Every energy = E hypersurface, for which $E > E_{thres}$, is split into two domains, A and B, representing the two "arrangements" of Ar_3 linked by the inversion process. Their projections onto configuration space, labeled in Fig. 2, are separated by a "dividing surface" at $q_1 = 0$. The configuration space dividing surface corresponds to two phase space transition states, S^a and S^b; S^a is associated with motion into A from B, while S^b is its time reversal. A reaction occurs when a phase space trajectory, satisfying Hamilton's equations, crosses from one domain to another.The chemically interesting features of this dynamics are the time scales for the transition process and the relative amount of time spent in each cell.

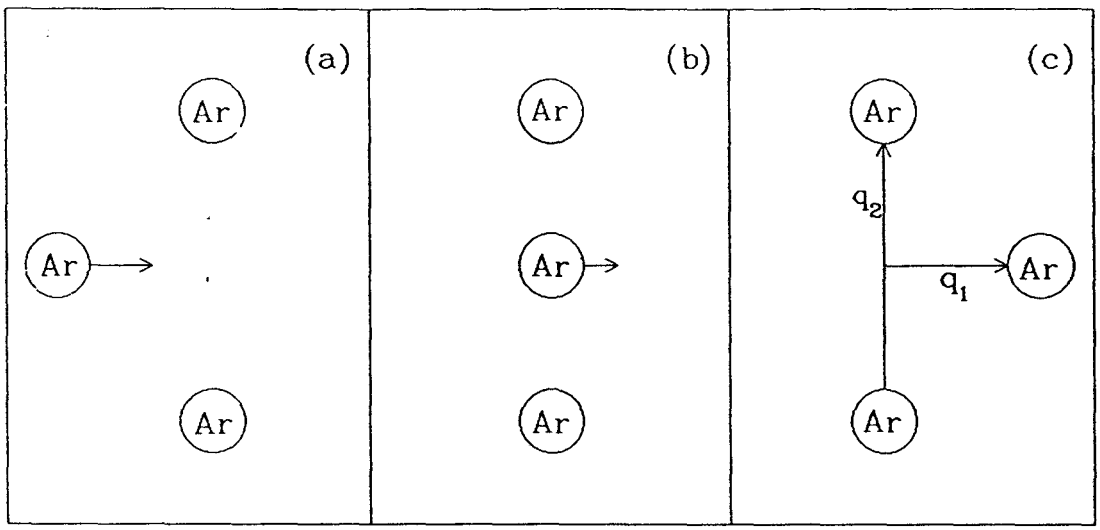

Fig. 1. The inversion process of T-shaped Ar_3. In T-shaped Ar_3, one of the argon atoms is constrained to move along the perpendicular bisector of the bond associated with the other two atoms. This constrained system has two degrees of freedom, q_1 and q_2, which are depicted in panel (c). The inversion process is illustrated in the succession of panels, (a), (b) and (c). In this process, the central argon passes from the left of the q_2 bond to its right [(a) to (c)]. The left and right "cells" are separated by the collinear transition state configuration of panel (b).

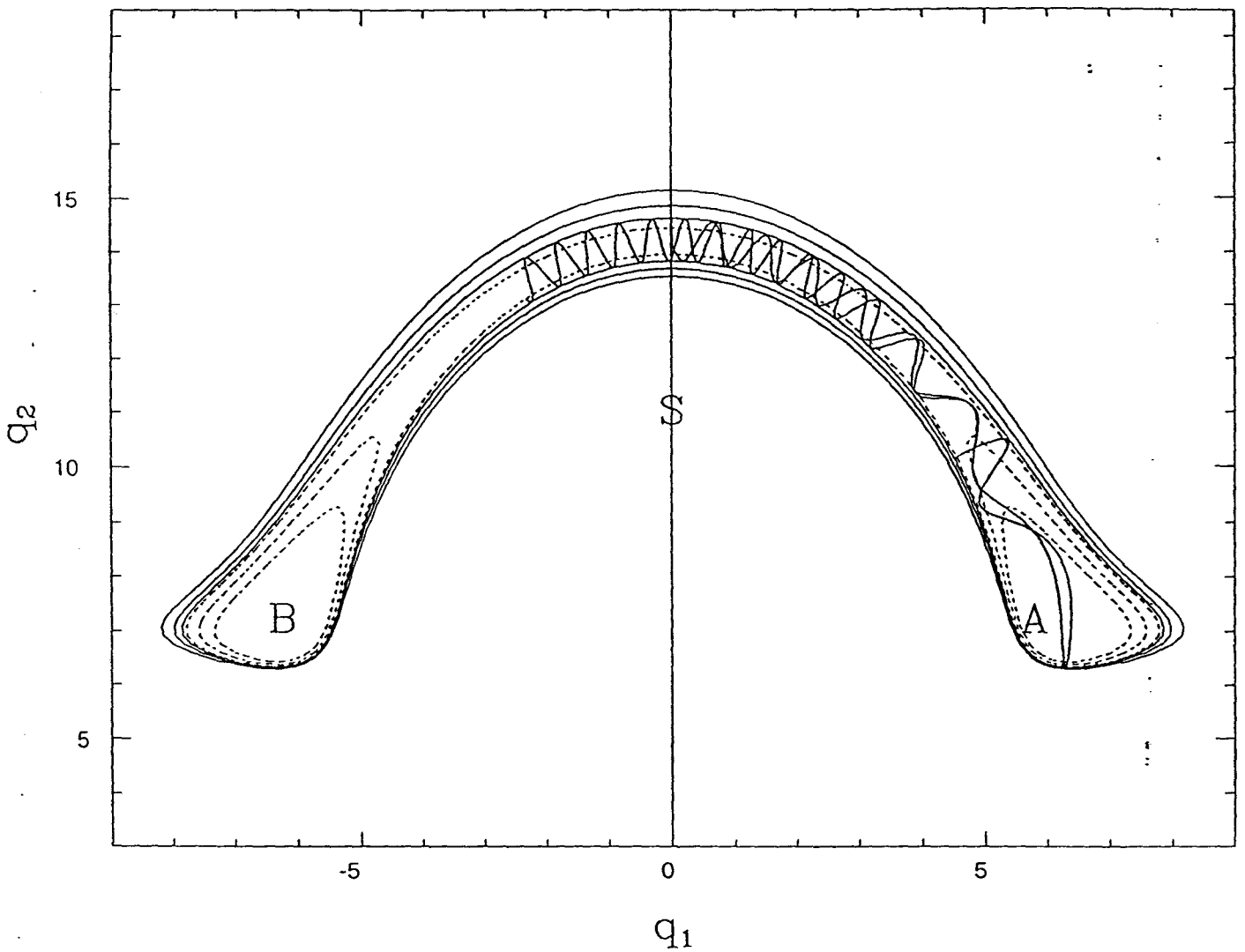

Fig. 2. Contour plot of T-shaped Ar_3 potential energy surface; E = 100 K, 125 K, 144 K, 150 K, 160 K and 175 K[13]. The three lowest energy contours are dashed, while the others are solid. The $q_1 = 0$ line (q_2-axis) divides $E > E_{thres}$ energy allowed wells into two domains, labeled A and B. They are associated with the two distinct arrangements of Ar_3, depicted in Fig. 1. Also shown is a typical E = 150 K trajectory which crosses the dividing surface.

In terms of the T-geometry restricted Jacobi coordinates of Fig. 2 , the two degree of freedom system Hamiltonian is given by

$$H(q,p) = \frac{p_1^2}{2m_1} + \frac{p_2^2}{2m_2} + V(q_1,q_2) \; . \qquad (2.1)$$

Here, m_1 and m_2 are reduced masses, $m_1 = 2m_{Ar}^2/(3m_{Ar}) = 2m_{Ar}/3 = 0.1539$ eH/K and $m_2 = m_{Ar}^2/(2m_{Ar}) = m_{Ar}/2 = 0.1154$ eH/K .[13d]

2.1 Survival Probability

The process of interest is the simple two-species isomerization, with chemical equation

$$A \rightleftharpoons B \qquad (2.2)$$

Classical isomerization dynamics is treated in two stages, preparation and evolution.

(1) First,there is the preparation stage where an initial ditribution of reactant species states is somehow created. We consider the case of an initial ensemble of species A alone. The only other constraint placed on this phase-space distribution is that it be associated with a single indecomposable[14] manifold, Γ ; i.e., the distribution is restricted to lie in a subset of phase space where the dynamics is necessarily ergodic[15]. This constraint ensures that it is not possible to break up the initial ensemble into subsets whose dynamics can be treated independently.

(2) The prepared initial distribution evolves in time according to Hamilton's equations of motion. The features of this evolution which are of chemical interest, are contained in the so-called "survival probability" or number-number correlation C(t):

$$C(t) = \langle a_t a \rangle / \langle a \rangle \qquad (2.3a)$$

Here, a is the characteristic function associated with species A,

$$a(x) = \begin{cases} 1, \text{ x is a state of species A} \\ 0, \text{ otherwise,} \end{cases} \tag{2.3b}$$

a_t is the time-evolved distribution function,

$$a_t(x) = a(x_{-t}) \tag{2.3c}$$

and <f> denotes the "Γ integral" of phase-space function f,

$$\langle f \rangle = \int_\Gamma d\mu(x)\, f(x) \tag{2.3d}$$

where μ is the invariant measure on the indecomposable invariant manifold, Γ.

The phenomenological description of the isomerization process by a chemical kinetics rate law implies that survival probability decays exponentially from unity at t = 0 to a long-time equilibrium value:

$$C(0) = 1 \tag{2.4a}$$

and

$$C(t) \to \langle a \rangle, \tag{2.4b}$$

as $t \to \infty$ where <a> is the microcanonical phase space "volume" associated with A. In Eq. (2.4b), we assume that invariant measure μ is normalized such that $\langle 1 \rangle = \mu(\Gamma) = 1$. This phenomenology has an important implication for the dynamics. Eq. (2.4b) holds only if the dynamics is mixing on Γ, since it has already been hypothesized to be ergodic.[15] The mixing assumption is essential if the dynamics is to exhibit relaxation of species populations

2.2 Reactive Flux

The reactive flux or number-flux correlation, K(t) is defined in terms of the surival probability:

$$K(t) = -dC(t)/dt \tag{2.5a}$$

$$= -\langle j_t a \rangle / \langle a \rangle, \tag{2.5b}$$

where, $j_t = da_t/dt$ is the "flux-density" associated with A. Flux density, j, can be separated into its positive and negative parts:

$$j(x) = j^b(x) - j^a(x) \qquad (2.6a)$$

where

$$j^b(x) = \begin{cases} j(x), & j(x) > 0, \\ 0, & \text{otherwise}, \end{cases} \qquad (2.6b)$$

and

$$j^a(x) = \begin{cases} -j(x), & j(x) < 0, \\ 0, & \text{otherwise}. \end{cases} \qquad (2.6c)$$

Since both $j^a(x)$ and $j^b(x)$ are positive functions, they provide densities for distributions of initial conditions in Γ just like a(x). The distribution associated with j^b is concentrated on S^b, while the j^a distribution is concentrated on S^a. These assertions are made by the following calculation. Since a(x) is a unit step function,

$$\begin{aligned} j(x) &= da(x_{-t})/dt\big|_{t=0} \\ &= -\, v(x).n(x)\, \delta^S(x), \end{aligned}$$

where $v(x_t) = dx_t/dt$ is the "phase-space velocity" at x_t, n(x) is the "incoming unit normal" to S at $x \in S$, and δ^S is a delta function concentrated on S. Therefore,

$$j^a(x) = v(x)\cdot n(x)\, \delta^{S^a}(x). \qquad (2.7a)$$

and

$$j^b(x) = -\, v(x)\cdot n(x)\, \delta^{S^b}(x). \qquad (2.7b)$$

For T-shaped Ar_3 with the configuration space dividing surface shown in Fig. 2, the transition state S^a is given by

$$\begin{aligned} S^a = \{x = (q,p) \,|\, & q = (0, q_2),\ p = (p_1 > 0, p_2) \\ & \& \ H(x) = E\}. \end{aligned} \qquad (2.8)$$

With the configuration space defined transition state of Eq. (2.8) , $v(x)\cdot n(x)$ is just the usual configuration space velocity in the q_1 direction.

Using Eq. (2.6a), Eq. (2.5b) can now be rewritten as :

$$K(t) = k_a \left(\langle j^a_t a\rangle/\langle j^a\rangle - \langle j^b_t a\rangle/\langle j^b\rangle\right), \tag{2.9}$$

where

$$k_a = \langle j^a\rangle/\langle a\rangle \tag{2.10}$$

is termed the "statistical decay rate" of the virtual unimolecular decomposition of arrangement A . Note that $\langle j^a\rangle = \langle j^b\rangle$ follows from time-reversal symmetry of S. Statistical rate, k_a is easily evaluated using Monte Carlo methods[16]. $\tau_a \equiv k_a^{-1}$ is the "mean gap time" associated with arrangement A ; i.e. the mean time to traverse the gap through A from S^a to S^b. It is the flux density weighted mean visitation time to region A , associated with energy = E trajectories.

2.3 Flux-Flux Correlation

For the purpose of present theoretical investigations , it is desirable to go one step further and work directly with the "flux-flux correlation", F(t) , instead of reactive flux:

$$F(t) = -\tau_a dK(t)/dt. \tag{2.11}$$

In order to provide an independent interpretation of F(t) , we backtrack and consider the second alternative form of reactive flux. Using the time translation invariance of μ and Γ , Eq. (2.9) can be expressed as

$$K(t) = \langle j^a a_{-t}\rangle/\langle a\rangle - \langle j^b a_{-t}\rangle/\langle a\rangle \tag{2.12}$$

The first and second terms on the right hand side of Eq. (2.12) are , respectively, the incoming (to A) and outgoing (from A) fluxes observed at time = -t, given an initial distribution uniform in A . Substitution of Eq. (2.12) into Eq. (2.11) (and using Eq. (2.10) for τ_a) gives :

$$F(t) = \langle j^a j_{-t} \rangle / \langle j^a \rangle - \langle j^b j_{-t} \rangle / \langle j^a \rangle \quad (2.13)$$

Using time translation invariance of μ and Γ, and Eq. (2.6a) , we get

$$F(t) = \langle j_t^a j^b \rangle / \langle j^a \rangle - \langle j_t^a j^a \rangle / \langle j^a \rangle$$
$$- \langle j_t^b j^b \rangle / \langle j^b \rangle - \langle j_t^b j^a \rangle / \langle j^b \rangle \quad (2.14)$$

Due to symmetry of T- shaped Ar_3 , Eq. (2.14) can be expressed in the following simpler form:

$$F(t) = 2[\langle j_t^a j^b \rangle / \langle j^a \rangle - \langle j_t^a j^a \rangle / \langle j^a \rangle] \quad (2.15)$$

The first and second terms in this expression have the interpretation of incoming and outgoing fluxes observed at time = t , subsequent to preparation at time = 0 of "incoming " or "outgoing" phase space distributions concentrated on S^a, respectively.

2.4 Numerical Computations

Three different energies, E =166 K, 150 K and 144 K are considered in the present work. Numerical computation of F(t) via Eq. (2.15) proceeds in two steps:

(i) First, a flux density ensemble of trajectories , denoted by $j^a/\langle j^a \rangle$, is initiated on S^a. General means of sampling the transition state according to flux density are described in Appendix A. The method was employed in all T-shaped Ar_3 computations presented here. It is an efficient Monte Carlo scheme which can be adapted to studies of more complex intramolecular processes associated with larger molecules.

(ii) Then trajectories are evolved according to Hamilton's equations and $j^a(x_t)$ is observed. This step is simplified by the fact that nonzero flux appears only at discrete times when x_t crosses S^a or S^b. The trajectories are propagated for time t_{max}, the longest time of interest. When a trajectory crosses S^b at time = $t_{cross} < t_{max}$ (i.e. it crosses the dividing surface heading into B), there is an $N^{-1}\delta(t - t_{cross})$ contribution to F(t) , where N is the number of trajectories in the ensemble. When it crosses S^a at

another time = t'_{cross} , there is a $[- N^{-1}\delta(t - t'_{cross})]$ contribution to the flux-flux correlation.

Reactive flux and survival probability are calculated from F(t) by successive integration. In Monte Carlo sampling of initial conditions , errors in F(t) at successive times are uncorrelated. This results in small errors in the corresponding estimates of K(t), and C(t) as well, since the many uncorrelated errors that are summed on integration, tend to cancel each other. Thus, the present scheme provides accurate and efficient numerical estimate of C(t).

To check the assumption of ergodicity on all energy = E hypersurfaces treated numerically in the present work, very long trajectories exhibiting approximately 10000 successive visits to A and B were computed. The mean visitation time provides a mean gap time associated with the minimal invariant manifold containing the trajectory. Its agreement with Monte Carlo determined mean gap time represents evidence for ergodicity on the energy hypersurface.

2.5 Results And Discussion:

Results of T-shaped Ar_3 flux-flux correlation computations are shown in Fig. 3 . Associated survival probabilities are provided in Fig. 4. The dot- dashed lines, in Fig. 4, are the corresponding statistical survival probabilities, consistent with a kinetics treatment of the simple isomerization mechanism (2.2). The statistical survival probabilities are just simple exponential decays to equilibrium. Specifically,

$$C_{stat}(t) = \frac{1}{2}[1 + \exp(-2k_a t)] \ . \qquad (2.16)$$

The observed survival probabilities begin falling off with the initial statistical rate of $2k_a$. However, their decay quickly becomes more rapid than statistical. Most notable, is the case of E = 160 K , which exhibits a nonstatistical "overshoot" of the

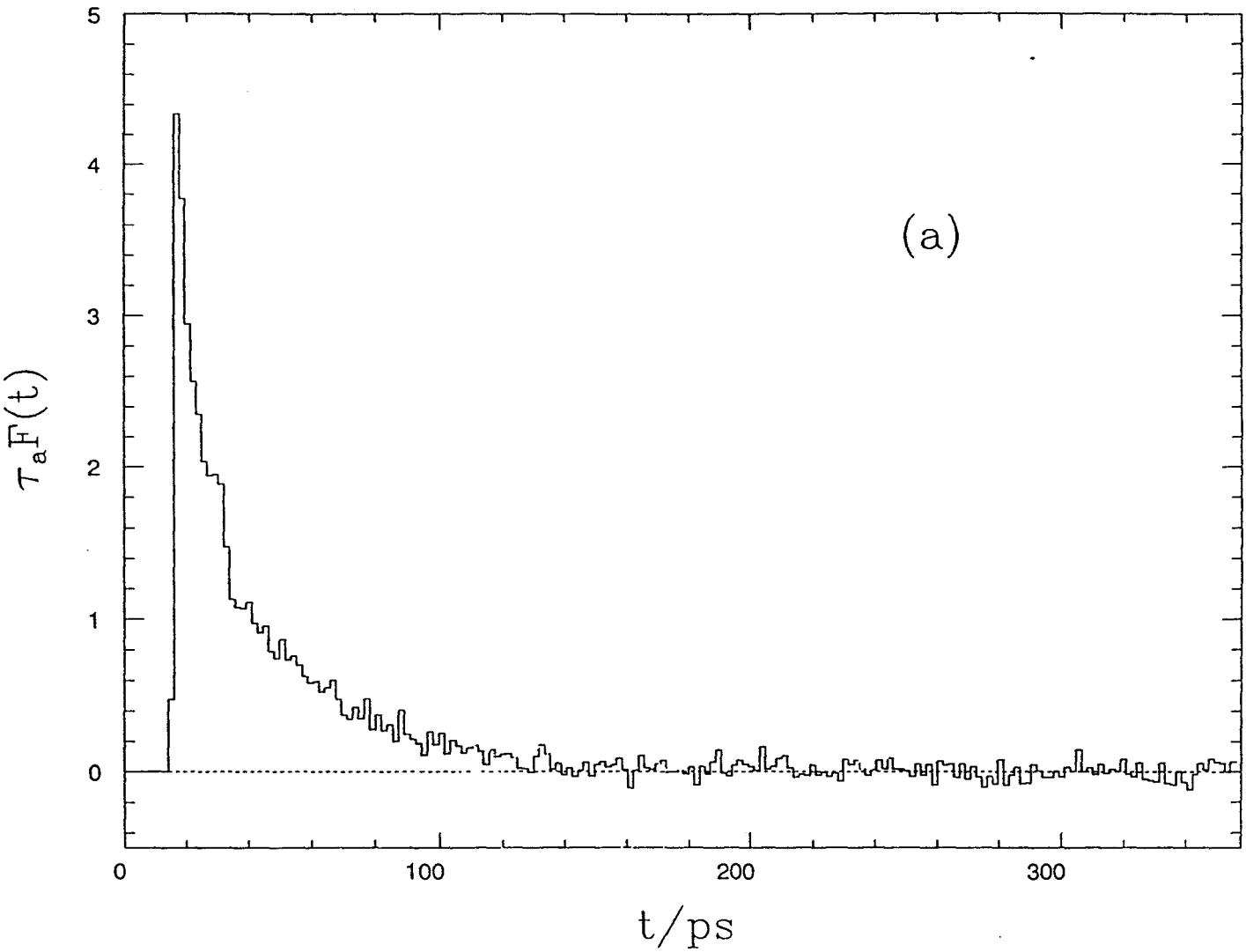

Fig. 3. T-shaped Ar_3 flux-flux correlation function at E = 144 K. The data are reported as histograms. The time resolution used is dt = 0.02 τ_a. 80,000 trajectories were computed. Associated mean gap time, τ_2 (determined to within 0.2% by Monte Carlo calculations) is given in Table 1.

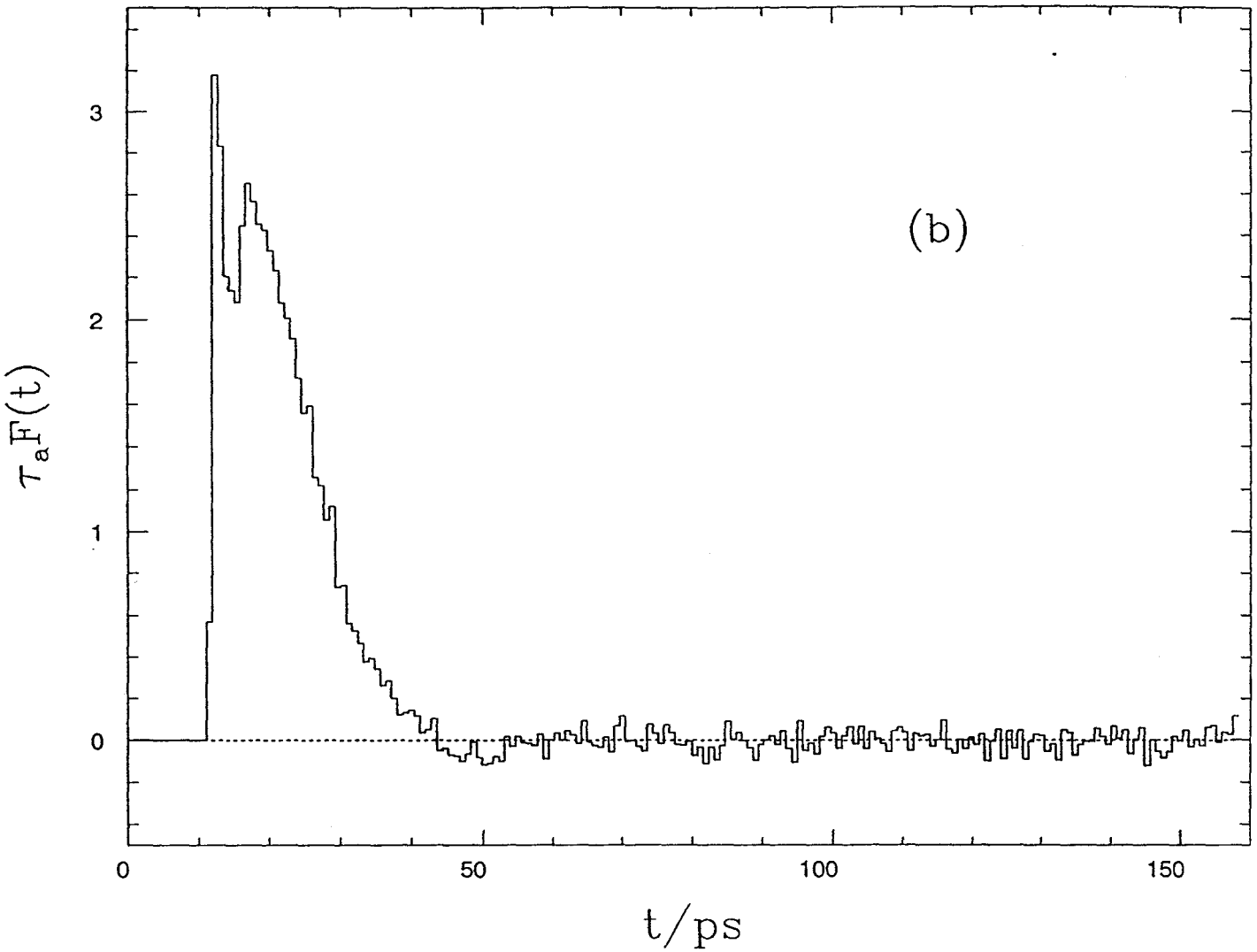

Fig. 3. T-shaped Ar_3 flux-flux correlation function at E = 150 K. The data are reported as histograms. The time resolution used is dt = 0.02 τ_a. 80,000 trajectories were computed. Associated mean gap time, τ_2 (determined to within 0.2% by Monte Carlo calculations) is given in Table 1.

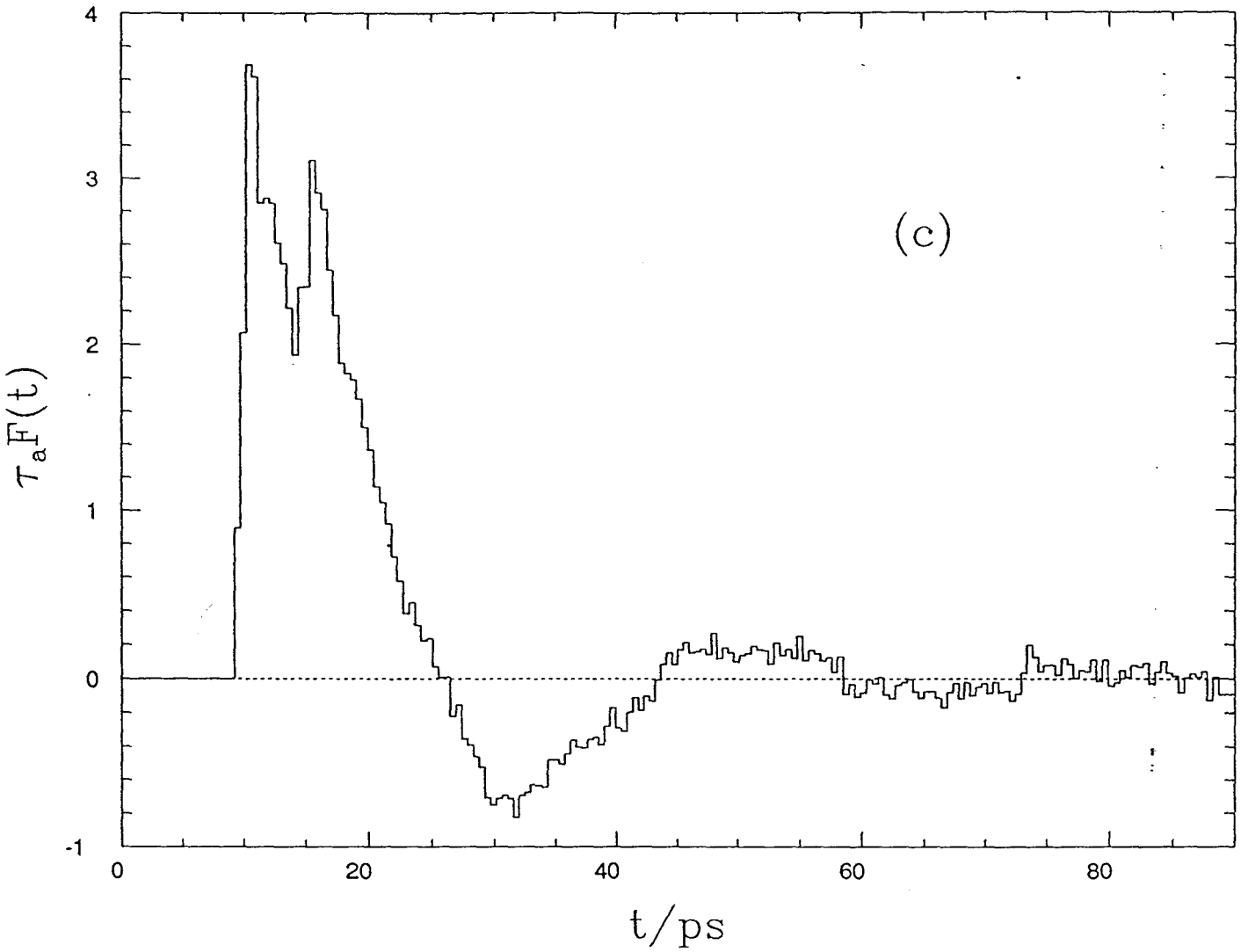

Fig. 3. T-shaped Ar_3 flux-flux correlation function at E = 160 K. The data are reported as histograms. The time resolution used is dt = 0.02 τ_a. 80,000 trajectories were computed. Associated mean gap time, τ_2 (determined to within 0.2% by Monte Carlo calculations) is given in Table 1.

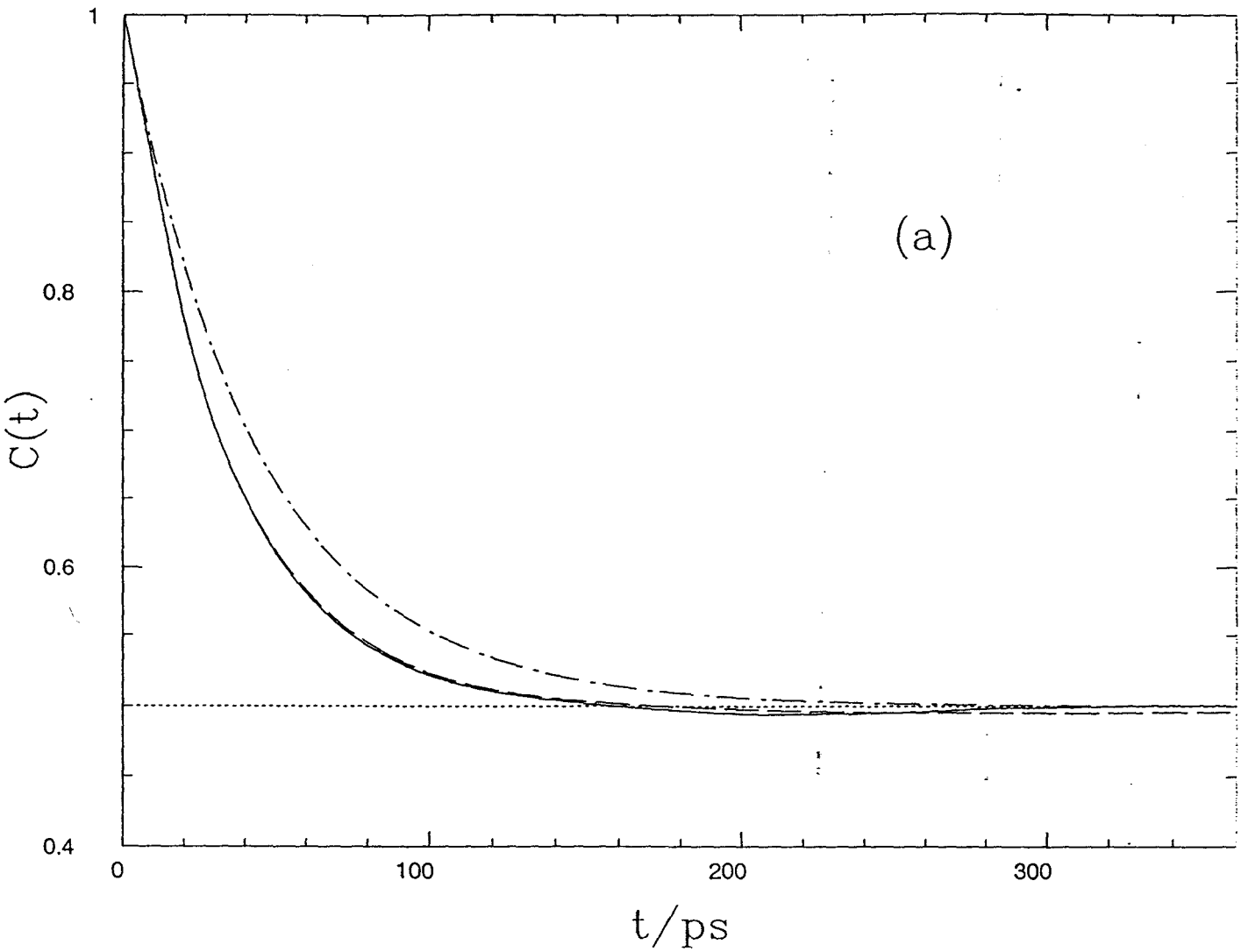

Fig. 4. Observed survival probability at E = 144 K (solid curve) corresponding to the flux-flux correlation of Fig. 3 (a). The dot-dashed curve shows associated fully statistical survival probability. The latter curve is consistent with simple inversion kinetics [see Eq. (2.16)]. The dashed curve shows absorbing barrier method model survival probability.

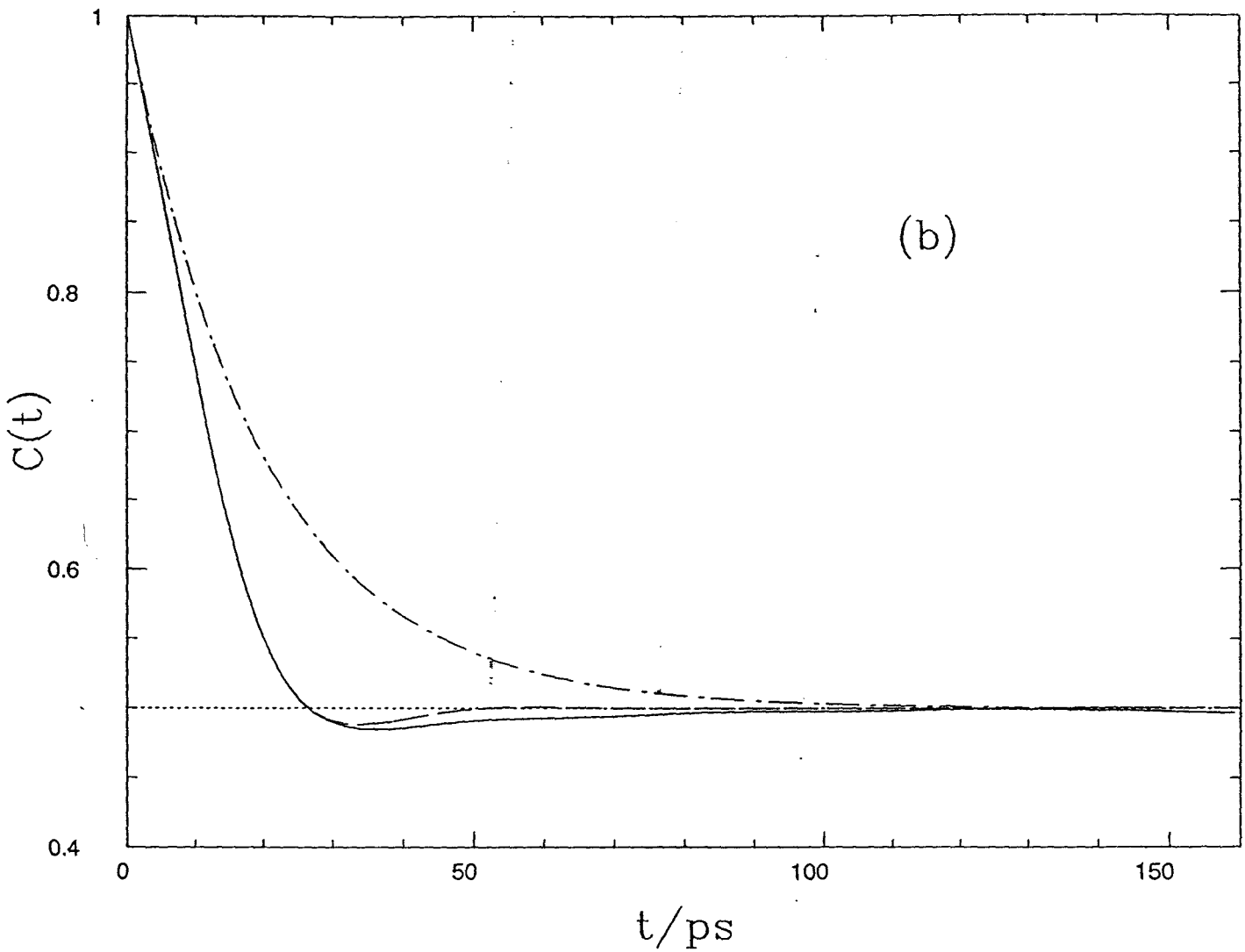

Fig. 4. Observed survival probability at E = 150 K (solid curve) corresponding to the flux-flux correlation of Fig. 3 (b). The dot-dashed curve shows associated fully statistical survival probability. The latter curve is consistent with simple inversion kinetics [see Eq. (2.16)]. The dashed curve shows absorbing barrier method model survival probability.

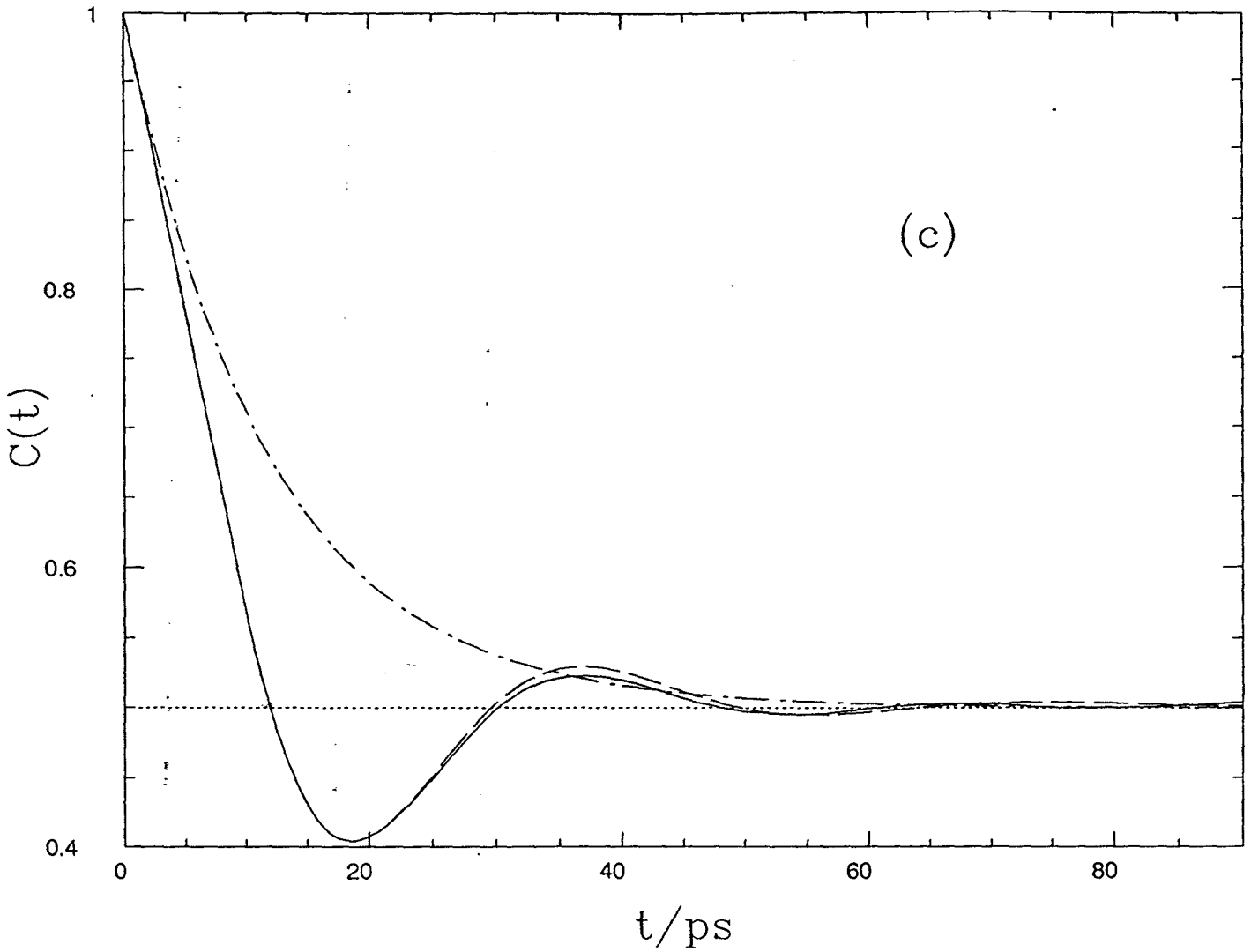

Fig. 4. Observed survival probability at E = 160 K (solid curve) corresponding to the flux-flux correlation of Fig. 3 (c). The dot-dashed curve shows associated fully statistical survival probability. The latter curve is consistent with simple inversion kinetics [see Eq. (2.16)]. The dashed curve shows absorbing barrier method model survival probability.

long time equilibrium population, and a subsequent oscillatory approach to equilibrium. The case of E = 150 K exhibits the overshoot, but no subsequent oscillations.

There is a marked contrast in the degree of nonstatisticality exhibited at the three different chosen energies. For example, the highest energy, E = 160 K , for which the inversion time scale is shortest, exhibits the greatest degree of nonstatisticality. This is in keeping with the principle that statistical behavior dominates when the time scale of the "reaction" process is much longer than those of competing processes, which contribute to nonstatistical behavior[17]. Thus, we rationalize the observed survival probabilities by proposing that there is an intrinsic motion of T-shaped Ar_3 , with time scale at most weakly dependent on energy, which competes with inversion and contributes nonstatisticality to the inversion dynamics. This motion is not very important at E = 144 K , where the inversion time scale is much longer than that of the competing process. However, at higher energies, where inversion is faster, the effects of the fast competing process are more significant.

Mean gap time(τ_1), obtained from very long trajectories exhibiting approximately 10000 successive visits to A and B, are given in Table 1, together with the mean gap time(τ_2), calculated using trajectories sampled from S^a, at three different energies. Associated microcanonical values of mean gap time(τ_3), obtained from Monte Carlo computations[16] using statistical formula based on ergodicity, is also given for comparision. Both τ_2 and τ_3 agree, to within computational error, suggesting that there are no Trapped Islands(T)[18] in phase space. If there were any , their microcanonical average $< T > \cong 0$, otherwise τ_2 would have been smaller than τ_3 .

Table 1. Mean gap times obtained by three different methods[a] at three different energies

energy	160 K	150 K	144 K
τ_1[b]/ps	23.34	39.42	91.17[d],90.4[e]
τ_2[c]/ps	23.14	39.57	89.87
τ_3/ps	23.22	39.56	89.06

(a) Methods are defined in the text.

(b) τ_1 is obtained to an accuracy of ~ 1 % ,exept at energy = 144 K, in which case an additional trial is made to get an accuracy of ~ 0.7 %.

(c) τ_2 is obtained to an accuracy of ~ 0.35 % .

(d) Mean gap time is obtained from 9777 successive visits to A and B.

(e) Mean gap time is obtained from 19721 successive visits to A and B.

Agreement of τ_1 with τ_3 confirms that there are almost no Crossing Islands[18], otherwise τ_1 would have been larger than τ_3. Thus the agreement of τ_1 and τ_2 with τ_3 constitutes support for our contention that, trajectories do not access T or $\dot{C}$ and T-shaped Ar_3 is ergodic (or very nearly so) at the energies considered. Specifically , the numerical results suggest that the chaotic minimal invariant manifolds occupy the bulk of their energy hypersurfaces(> 99% of microcanonical invariant measure). However it must be pointed out that , our assumption of ergodicity and its numerical support notwithstanding, T-shaped Ar_3 cannot be ergodic at the energies considered here, or any other energy. No generic Hamiltonian system, such as this one, is strictly ergodic[19]. The single trajectory computation of mean gap time, together with the Monte Carlo mean gap time computations, are interpreted as evidence for a very small total relative size of regular "KAM regions", in the energy hypersurfaces in question. The assumption of ergodicity is viewed only as a good approximation, useful in simplifying theoretical formulae.

The above interpretation of the observed nonstatistical survival probabilities is further elaborated in Chapter 4. Before proceeding along those lines, however , we attempt to model the observed survival probabilities with the absorbing barrier method in Chapter 3.

Chapter 3

Absorbing Barrier Method

Chapter 3

Gap Distributions and the Absorbing Barrier Method

The absorbing barrier method provides a statistical model expression for the flux-flux correlation in terms of "gap distributions" associated with phase space regions, A and B . Its derivation begins with Eq. (2.15), which expresses F(t) in terms of elementary correlations of the form

$$F^{ab} = \langle j_t^a j^b \rangle / \langle j^a \rangle. \tag{3.1}$$

It is possible to decompose these correlations into even more elementary components . For example[5c],

$$F^{ab}(t) = \sum_{j=1}^{\infty} P_j^{ab}(t), \tag{3.2}$$

where $P_j^{ab}(t)$ is the probability distribution for the j th transit time from S^a to S^b . Eq. (3.2) shows that computation of F(t) requires determination of all transit times from S^a and S^b to S^a and S^b. Such a computation is simplified considerably if the dynamics in A and/ or B is sufficiently chaotic to eliminate correlations between successive first transit times (or gap times). This is because a jth transit time is the sum of 2j or 2j-1 successive gap times. If all successive gap times are independent, then the jth transit time distribution can be expressed in terms of gap distributions. For example,

$$P_j^{ab}(t) = (P_a * P_b * P_a \cdots * P_a)(t),$$

$$\leftarrow j\ P_a\text{'s}\rightarrow \qquad (3.3)$$

where,

$$P_a(t) = P_1^{ab}(t)$$

and

$$P_b(t) = P_1^{ba}(t)$$

are the A and B gap distributions, respectively, and * denotes convolution,

$$(P_a * P_b)(t) = \int_0^t dt' P_a(t') P_b(t - t')$$

Eq. (3.3) constitutes the absorbing barrier method. It provides F(t), via Eqs. (2.15) and (3.2), in terms of gap distributions alone. Since only first transit times need to be computed, S acts as an absorbing barrier; i.e., we terminate each trajectory when it returns to S for the first time. In other words, it is absorbed by an "absorbing barrier" at the transition state.

In practice, the Fourier (or Laplace) transform of Eq. (3.3) is used:

$$P_j^{ab}(\omega) = P_a^{\,j}(\omega)\, P_b^{\,j-1}(\omega)\,, \qquad (3.4)$$

where

$$P(\omega) = \int_0^\infty dt\, \exp(-i\omega t)\, P(t).$$

In terms of Fourier transforms , Eq. (3.1) takes the form,

$$F^{ab}(\omega) = \sum_{J=1}^{\infty} P_a^j\, P_b^{j-1}$$

$$= P_a \sum_{J=0}^{\infty} (P_a P_b)^j$$

$$= P_a(\omega)/\,[1 - P_a(\omega)\, P_b(\omega)], \qquad (3.5)$$

while the ABM flux-flux correlation is given by [see Eq. (2.15)]

$$F(\omega) = 2[F^{ab}(\omega) - F^{aa}(\omega)]$$
$$= 2\,P_a(\omega)[1 - P_a(\omega)]/[1 - P_a^2(\omega)] \qquad (3.6a)$$

or

$$F_{ABM}(t) = \mathcal{F}^{-1}\left[\frac{2\,P_a(\omega)\,[1 - P_a(\omega)]}{1 - P_a^2(\omega)}, \omega \to t\right] . \qquad (3.6b)$$

where, $\mathcal{F}^{-1}$ denotes inverse Fourier transformation.

The inversion of T-shaped Ar_3 is well described by the ABM. This is illustrated in Fig. 4, where ABM model C(t) data is shown, together with observed survival probabilities. The ABM clearly captures the essential features of the inversion dynamics. In particular, the ABM describes T-shaped Ar_3 inversion much better than it describes the siamese stadium billiard model isomerization[5c]. It appears that the statistical independence assumption, underlying the ABM is appropriate in the case of T-shaped Ar_3 . The trouble with the ABM, however, is that it does not provide a model gap distribution. Consequently, the ABM does not fully explain the nonstatisticality of observed survival probabilities. Rather, it associates the nonstatisticality with properties of the gap distribution, which in turn is obtained by explicit trajectory computation. To explain observed survival probabilities, we must correctly model associated gap distributions.

The E = 150 K gap distribution is shown in Fig. 5 . It exhibits a long delay during which there are no gap times. This delay is the source of nonstatisticality in the E = 150 K survival probability. The E = 144 and 160 K distributions show similar delays. However, the mean gap time of 89.17 ps at 144 K is so much larger that the delay time of $\simeq$ 16 ps is relatively negligible. In contrast, the delay time of $\simeq$ 10 ps dominates the E = 160 K gap distribution for which mean gap time

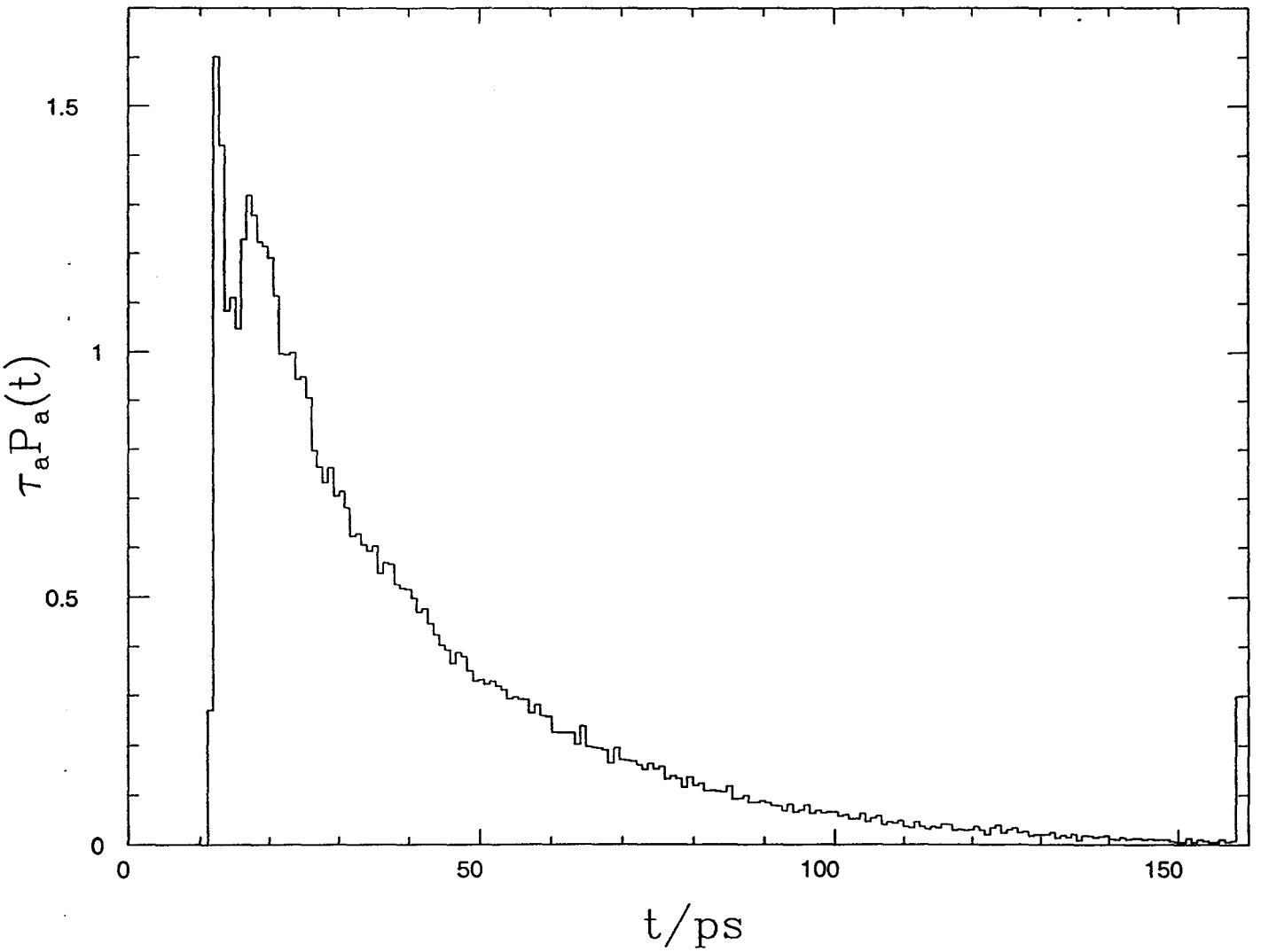

Fig. 5. E = 150 K gap distribution.

τ_a(E = 160 K) = 23.15 ps . The size of the delay time, relative to the mean gap time, determines the degree of survival probability nonstatisticality. This is demonstrated further, in Chapter 4, where a model gap distribution is combined with the absorbing barrier method [i.e. Eq. (3.6)]. The observed survival probabilities are described there in terms of a realistic model gap distribution which incorporates an appropriate internal delay time (or times).

A delay is a characteristic of the "delayed lifetime gap model" gap distribution (see Chapter 4 and Ref. 5a). However, the delay observed in the E = 150 K gap distribution is too long to be identified with the DLGM delay time. It is shown, further in Chapter 4, that the DLGM, in existing formulations, cannot describe T-shaped Ar_3 gap distributions. The DLGM is adapted, in the same chapter, to overcome this shortcoming, however.

The source of the long delay time can be seen by examining the T-shaped Ar_3 potential well (see Fig. 2). This well possesses a long, approximately separable, "neck" region about the transition state saddle point which reacting trajectories must traverse at the beginning and end of visitations to A and B . From a kinetics point of view, the observed nonstatistical survival probabilities might be understood, qualitatively, in terms of the following variation of the mechanism of Eq. (2.2):

$$\begin{array}{ccccc} & & N^+ & & \\ & \nearrow & & \searrow & \\ A & & & & B \\ & \nwarrow & & \swarrow & \\ & & N^- & & \end{array} , \qquad (3.7)$$

Here, N^+ and N^- correspond to motion of Ar_3 in the neck region of the potential surface, heading to the right and left, respectively. A kinetics treatment of this mechanism can produce oscillatory population time dependence, such as that observed at E = 160 K [see Fig. 4(c)], since the mechanism does not satisfy microscopic reversibility. Mechanisms satisfying microscopic reversibility are never associated with

oscillatory populations. Eq. (3.7) does not satisfy microscopic reversibility because it is not consistent with the principle of detailed balance. This results because phase space cells, N^+ and N^-, are not time reversal invariant[20]. In particular $N^+ \rightarrow N^-$ under time reversal.

Rather than adopting a kinetics treatment which might provide a phenomenological description of observed survival probability nonstatisticality, we seek a more detailed model gap distribution which incorporates explicit dynamical information and is based on well-founded assumptions of chaos. Specifically, we seek a model in the spirit of the delayed lifetime gap model. The result is an adaptation of the DLGM (Chapter 4). The new model accommodates the neck region by incorporating an additional delay at the beginning and the end of every gap time. The additional delay essentially achieves the effects of the mechanism of Eq.(3.7), while the use of the DLGM accounts for finitely rapid intramolecular relaxation.

Chapter 4

Adaptation of the Delayed Lifetime Gap Model

Chapter 4

4.1. Adaptation of the Delayed Lifetime Gap Model

The delayed lifetime gap model is a statistical theory of the gap distribution which can be applied to simple decomposition processes, or to isomerizations in conjunction with the absorbing barrier method. Ideas associated with the DLGM can also be used to go beyond the independence of successive gap times approximation of the ABM[5d]. However,this level of sophistication is not required here, since correlation of successive gap times is not a significant source of nonstatisticality in T-shaped Ar_3 inversion dynamics. Our strategy is to employ the ABM, and to consider the DLGM as a model of the required gap distributions.

DLGM is based on the relationship between the gap and lifetime distributions of unimolecular decompositions[5a]. The lifetime distribution associated with species A is defined by

$$P^a(t) = k_a \int_t^\infty dt' \, P_a(t'). \tag{4.1}$$

The DLGM for species A results from the imposition of a second relationship between the gap and lifetime distributions:

$$P_a(t) = P^a(t-\tau), \tag{4.2}$$

i.e. the gap distribution is just a delayed (by "intra-A relaxation time", τ) version of the lifetime distribution. Eq. (4.2) follows from a strong mixing condition. It corresponds to

the complete relaxation, within A, of incoming trajectories after evolution through time τ, which is both relaxation time and smallest gap time. However, in general, the smallest gap time does not coincide with the relaxation time. This gives rise to the DLGM decomposition of a gap distribution into "direct" and "strong collision" components[5]:

$$P_a(t) = f^{\alpha} P_{\alpha}(t) + f^{A} P_A(t) \ , \qquad (4.3)$$

Here Eq. (4.2) is satisfied by the gap and lifetime distributions associated with the strong collision component. f^{α} and $f^{A} = 1 - f^{\alpha}$ are the fractions of flux through S^a associated with the direct and strong collision components, respectively.

The direct gap distribution, $P_{\alpha}(t)$, is the gap time distribution associated with trajectory segments through A which are insufficiently "relaxed" to warrant statistical treatment. Therefore, $P_{\alpha}(t)$ is computed explicitly. Direct and strong collision trajectory segments are distinguished by their "divergence"; i.e. the factor by which an infinitesimal displacement of the trajectory is expanded during traversal of A . If the divergence is less than some predetermined relaxation threshold value, D , then the trajectory segment is labeled direct. Otherwise, it is part of the strong collision component. In the DLGM, the strong collision component gap distribution, $P_A(t)$, is treated using a statistical assumption[5a]. The DLGM is obtained by replacing $P_A(t)$ in Eq. (4.3) with the solution to the following delay differential equation:

$$dP_A(t)/dt = - k_A P_A(t-\tau) \qquad (4.4)$$

This Equation is satisfied by $P_A(t)$, only for $t = \tau$ to $t = \infty$. Here $k_A = 1/\tau_A$ is the reciprocal mean strong collision gap time

$$\tau_A = (\tau_a - f^{\alpha} \tau_{\alpha})/f^{A} \qquad (4.5)$$

and τ_{α} is the mean direct gap time. Eq. (4.4) follows from Eqs. (4.1) and (4.2) , applied to the strong collision component. The DLGM model replaces explicit computation of

$P_A(t)$ with a statistical approximation, given here in terms of the Fourier transform[8b] of the distribution:

$$P_{A,DLGM}(\omega) \equiv \int_0^\infty dt \exp(-i\omega t)\, P_{A,DLGM}(t) \qquad (4.6)$$

To get the expression for $P_{A,DLGM}(\omega)$, we take the Fourier transform of Eq. (4.4) :

$$\int_\tau^\infty \exp(-i\omega t)\, \dot{P}_A(t)\, dt = -k_A \int_\tau^\infty P_A(t-\tau)\exp(-i\omega t)\, dt.$$

Integrating by parts gives:

$$[\exp(-i\omega t)\, P_A(t)]_\tau^\infty + i\omega \int_\tau^\infty \exp(-i\omega t)\, P_A(t)\, dt$$

$$= -k_A \int_0^\infty P_A(t') \exp(-i\omega(t'+\tau))\, dt'$$

Here, $P_A(\tau) = k_A$ and the lower limit in the second term on left hand side can be changed to zero, since $P_A(t) = 0$ for $t < \tau$. Using Eq. (4.6) for $P_A(\omega)$, we get

$$\exp(-i\omega\tau)\, k_A + i\omega\, P_A(\omega) = -k_A \exp(-i\omega\tau)\, P_A(\omega)$$

or,

$$P_A(\omega) = 1/[1 + i\omega\, \tau_A \exp(i\omega\tau)] \qquad (4.7)$$

In an application of the DLGM, f^α, τ_α and $P_\alpha(t)$ are determined by explicit trajectory computation of the direct component. The DLGM relaxation time, τ, must be supplied independently. It is closely related to the divergence threshold, D , which is most appropriate for modeling the data. The latter quantity must also be supplied independently.

We test applicability of the DLGM to T-shaped Ar_3 inversion via computations of direct component properties, $P_\alpha(t)$, f^α and τ_α . These are used to evaluate τ_A , with Eq. (4.5), and $P_A(t)$, by inverting Eq. (4.3). The DLGM is tested by comparing the computed $P_A(t)$ with its associated lifetime distribution,

$$P^A(t) = k_A [1 - \int_0^t dt_1 P_A(t_1)] , \qquad (4.8)$$

where $k_A = 1/\tau_A$ is the strong collision statistical rate constant. The model strong collision gap distribution of Eq. (4.6) is related to its lifetime distribution by

$$P_{A,DLGM}(t) = P^A_{DLGM}(t-\tau) . \qquad (4.9)$$

A simple visual comparison of computed $P_A(t)$ and $P^A(t)$ determines the degree to which Eq. (4.9) is satisfied and $P_A(t)$ is consistent with the DLGM.

Figure 6 shows E = 150 K strong collision gap and lifetime distributions, $P_A(t)$ and $P^A(t)$, for D = 10^3, 10^4 and 10^5. The long delay at shorter times, where $P_A(t)$ is essentially zero, gives rise to a long $P^A(t) = k_A$ plateau [see Eq. (4.8)]. If the DLGM is to apply, then $P_A(t)$ should have a plateau of the same height shifted in time by τ [see Eq. (4.9)]. This requires τ to equal the gap distribution delay, or shortest gap time. It also requires, according to Eq. (4.8), τ to determine the width of the $P^A(t)$ plateau. The observed strong collision gap distributions can be roughly fitted with plateaus beginning at $t = \tau$. However, these plateaus are too high to be consistent with the DLGM. They are greater than k_A which is necessarily the height of the lifetime distribution. Furthermore, these plateaus are not as wide as corresponding lifetime distribution plateaus.

We understand the failure of the DLGM in this case by recalling that the DLGM is based on observations of ideally chaotic model dynamics[11]. Specifically, the model systems on which the DLGM is based are characterized by uniform instability and a single global relaxation time. In contrast, T-shaped Ar_3 dynamics has nonuniform instability. For example, very little divergence accumulates when trajectories are in the neck region of the potential well. This is because the potential is approximately separable in this region.

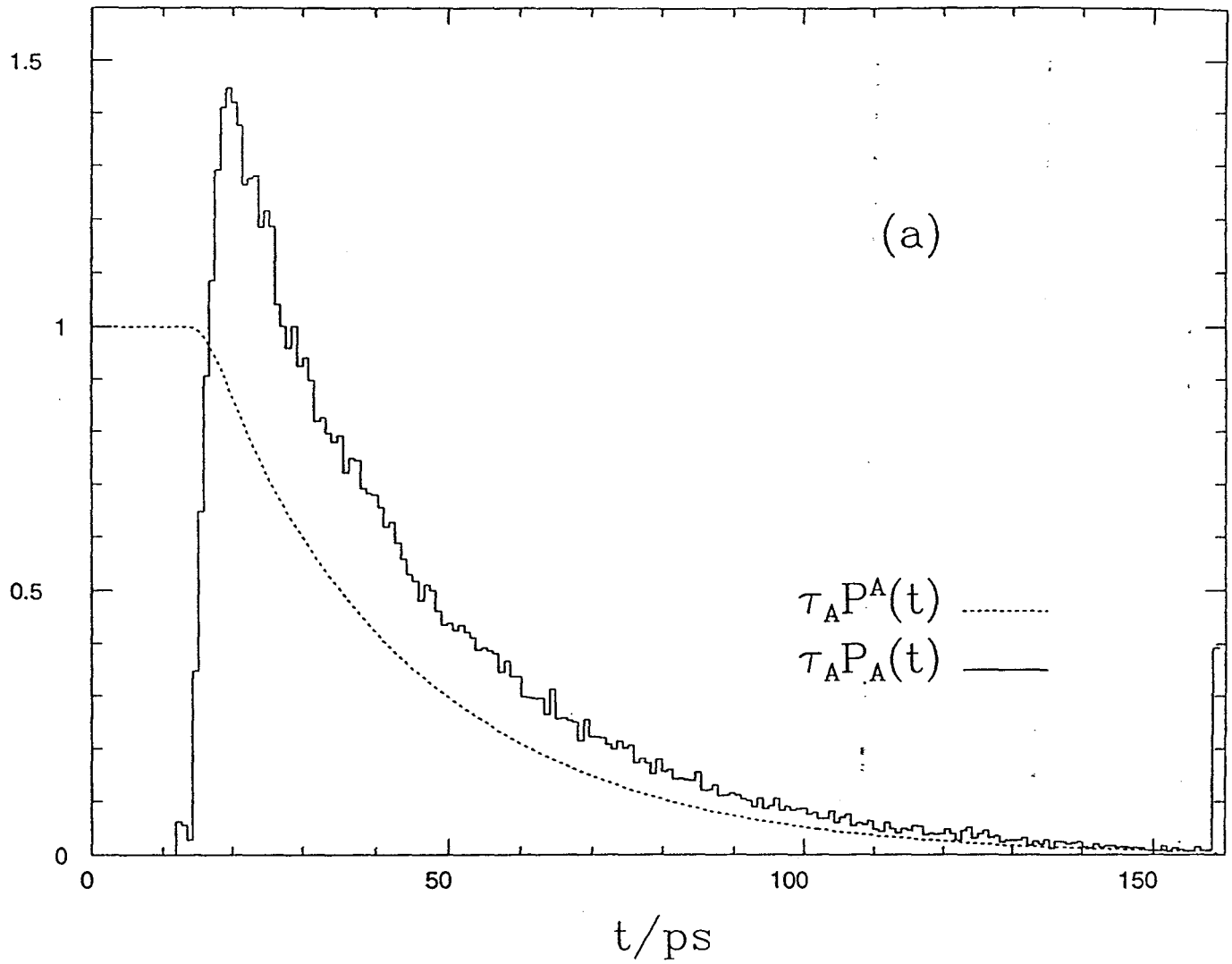

Fig. 6. E = 150 K strong collision gap and lifetime distributions. Associated divergence thresholds is 10^3. Lifetime distribution is shifted by τ as indicated.

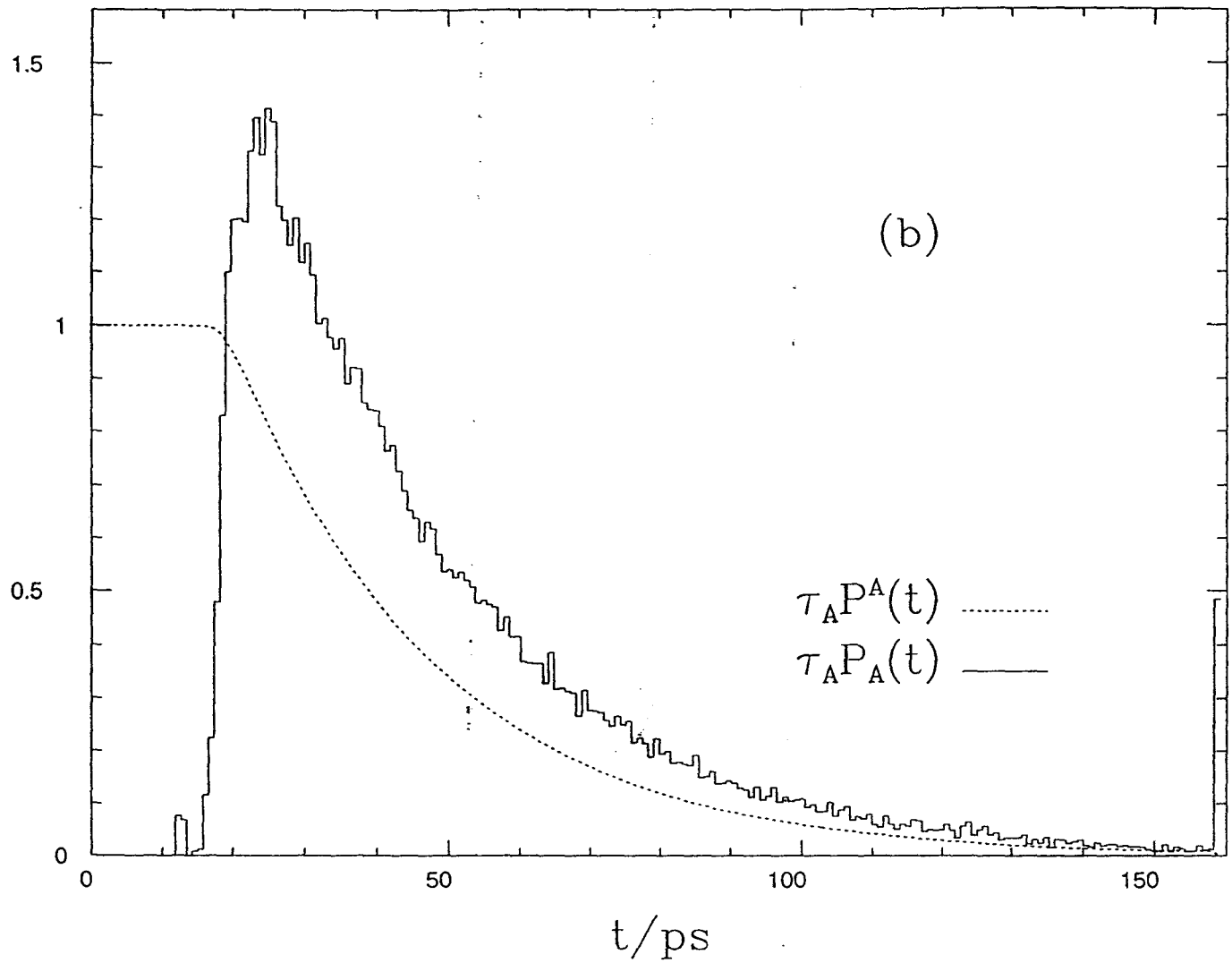

Fig. 6. E = 150 K strong collision gap and lifetime distributions. Associated divergence thresholds is 10^4. Lifetime distribution is shifted by τ as indicated.

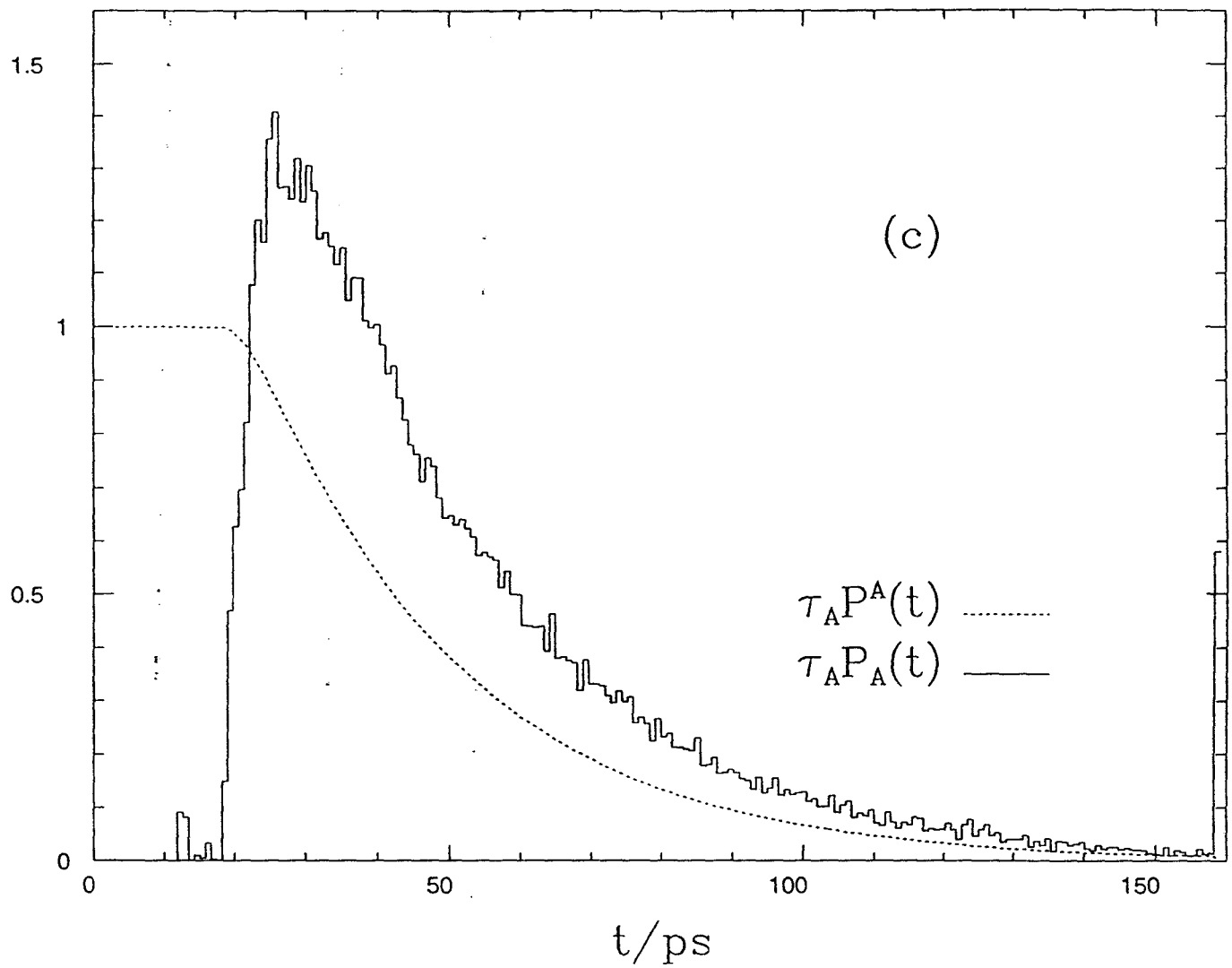

Fig. 6. E = 150 K strong collision gap and lifetime distributions. Associated divergence thresholds is 10^5. Lifetime distribution is shifted by τ as indicated.

Nonuniform exponential divergence has been encountered before in studies of open stadium billiard systems[5b,11]. In these applications, the DLGM was found to account for observed gap distributions if the regions of low instability were somehow removed from the stadium phase space. Two types of open stadium were considered. For one type of open stadium, the region of low instability was associated with the direct component of the decay, and it was removed by the DLGM separation of direct and strong collision components. In this case, the DLGM described the observed gap distribution without adaptation. The other open stadium billiard considered could not be treated by a straightforward application of the DLGM, since its region of low instability was not associated with direct component trajectories. The treatment of this system required adoption of an alternate reaction mechanism, with decay in explicit competition with transition into and out of the region of low instability. The region of low instability was thereby separated from the remainder of the decaying open stadium reactant phase space. The latter region was then subject to a DLGM treatment. The gap distribution within the region of low instability was computed explicitly and incorporated into the overall dynamics via an ABM-style "independence of successive gap times" assumption.

The T-shaped Ar_3 inversion region of low instability is encountered by all trajectories at the beginning and end of every visit to A. This is unlike either of the open stadium systems previously treated. However, T-shaped Ar_3 inversion can be modeled in terms of a simple adaptation of the DLGM.

The adapted delayed lifetime gap model presented here does not make direct use of the mechanism of Eq. (3.7). However, it does explicitly account for transit through the neck region. This account is accomplished by the introduction of an additional delay time, δ. The additional delay represents a typical time spent in the

neck region during a single visit to A. We envision the delay as split into two equal parts. Half of the delay is associated with the initial time spent in the neck region, while the other half represents time spent in the neck just prior to exit from A. The essential simplification introduced here is the use of a single time, δ, to represent neck region delay for all strong collision trajectories at a given energy.

It is very easy to implement the adaptation of the DLGM. All that is required is a reasonable value for the delay time. To determine such a value, we note that the delay is introduced in order that the DLGM might describe the gap distribution which results if the delay is subtracted from every gap time. Thus, we examine characteristics of such a gap distribution. Clearly, the only effect on the gap distribution which results from this effective removal of the neck region is a simple translation, or shift, in time. The lifetime distribution experiences both a shift and a renormalization. The latter effect is linked to the shift of the mean gap time. Note that a shift of all gap times is accompanied by the same shift of the mean gap time. The effect on the lifetime distribution is apparent from Eq. (4.8).

The effects of a delay on the gap and lifetime distributions are summarized as follows:

$$\tilde{P}_A(t) = P_A(t+\delta) , \tag{4.10a}$$

has associated mean, $\tilde{\tau}_A = \tau_A - \delta$, and

$$\tilde{P}^A(t) = (\tau_A/\tilde{\tau}_A)\, P^A(t+\delta) . \tag{4.10b}$$

Note that these equations are only valid if there are no gap times smaller than δ. This is a reasonable restriction, since δ represents time spent in the neck region by all trajectories. If every trajectory spends δ in the neck region of A, then none can have a gap time less than δ. The requirement that δ be less than the smallest gap time is not

difficult to satisfy here, since we are dealing with the strong collision component for which there are no short gap times.

If $\tilde{P}_A(t)$ is to be described by the DLGM, then its plateau value must match that of $\tilde{P}^A(t)$. This is the condition which is not met by the observed $P_A(t)$ and its associated lifetime distribution. From Eq. (4.10), it is easy to see that one can ensure coincidence of the shifted gap and lifetime distribution plateaus by choosing δ such that

$$(\tau_A/\tilde{\tau}_A)\, P^A_{plat} = P_{A,plat} \,, \tag{4.11a}$$

where $P_{A,plat}$ and $P^A_{plat} = k_A \equiv 1/\tau_A$ are the non-matching plateau values of the unshifted gap and lifetime distributions, respectively. Specifically, we choose δ according to

$$\begin{aligned} \delta &= \tau_A\,(1 - P^A_{plat}/P_{A,plat}) \\ &= \tau_A - 1/P_{A,plat} \,. \end{aligned} \tag{4.11b}$$

Equations (4.10) and (4.11) determine shifted gap and lifetime distributions, $\tilde{P}_A(t)$ and $\tilde{P}^A(t)$, for the three D values already considered. The plateau values employed are determined by examination of Fig. 6. They are provided in Table 2. Applicability of the DLGM to the shifted gap distribution is tested by comparing $\tilde{P}_A(t)$ to $\tilde{P}^A(t-\tau)$, with an appropriate choice for τ. The results of such tests are shown in Fig. 7. The DLGM τ values are chosen to give the best possible agreement between $\tilde{P}_A(t)$ and $\tilde{P}^A(t-\tau)$. These and other parameters associated with the data are summarized in Table 2. The figure shows rather good agreement between $\tilde{P}_A(t)$ and $\tilde{P}^A(t-\tau)$, particularly for D = 10^4 and 10^5. Other requirements necessary for validity of the delayed lifetime gap model are tested as follows:

(1) The DLGM lifetime distribution has a plateau of width τ. To see how well τ approximates the width of the observed lifetime distribution plateaus, we have placed

Table 2. Parameters associated with adapted delayed lifetime gap modeling of E = 150 K T-shaped Ar_3 gap distribution.[a] Times are reported here in ps . Note that τ_a = 39.6 ps .

D	10^3	10^4	10^5
τ_A/ps	44.1	47.7	50.8
$\tau_A P_{A,plat}$ [b]	1.42	1.35	1.35
δ/ps [c]	12.7	11.9	12.7
τ/ps [c]	4.2	6.5	8.2
τ_{gap}/ps [d]	27.9	28.0	27.9
τ_{life}/ps [d]	28.4	28.4	28.4
$\tilde{\tau}_{DLGM}$/ps [e]	26.9	28.5	28.7

[a] Parameters are defined in the text.

[b] Appropriate plateau values were extracted from Fig. 6 . Note that $P^A_{plat} = k_A = 1/\tau_A$.

[c] δ is obtained from Eq. (4.11b), then rounded to the the nearest multiple of the time resolution, dt . τ is similarly rounded.

[d] τ_{gap} and τ_{life} are exponential time constants obtained from least square fits of strong collision gap and lifetime distribution log data. The range of times employed in the fittings is given by 21 ps < t < 140 ps .

[e] $\tilde{\tau}_{DLGM}$ is the adapted DLGM exponential time constant, obtained from Eq. (4.12).

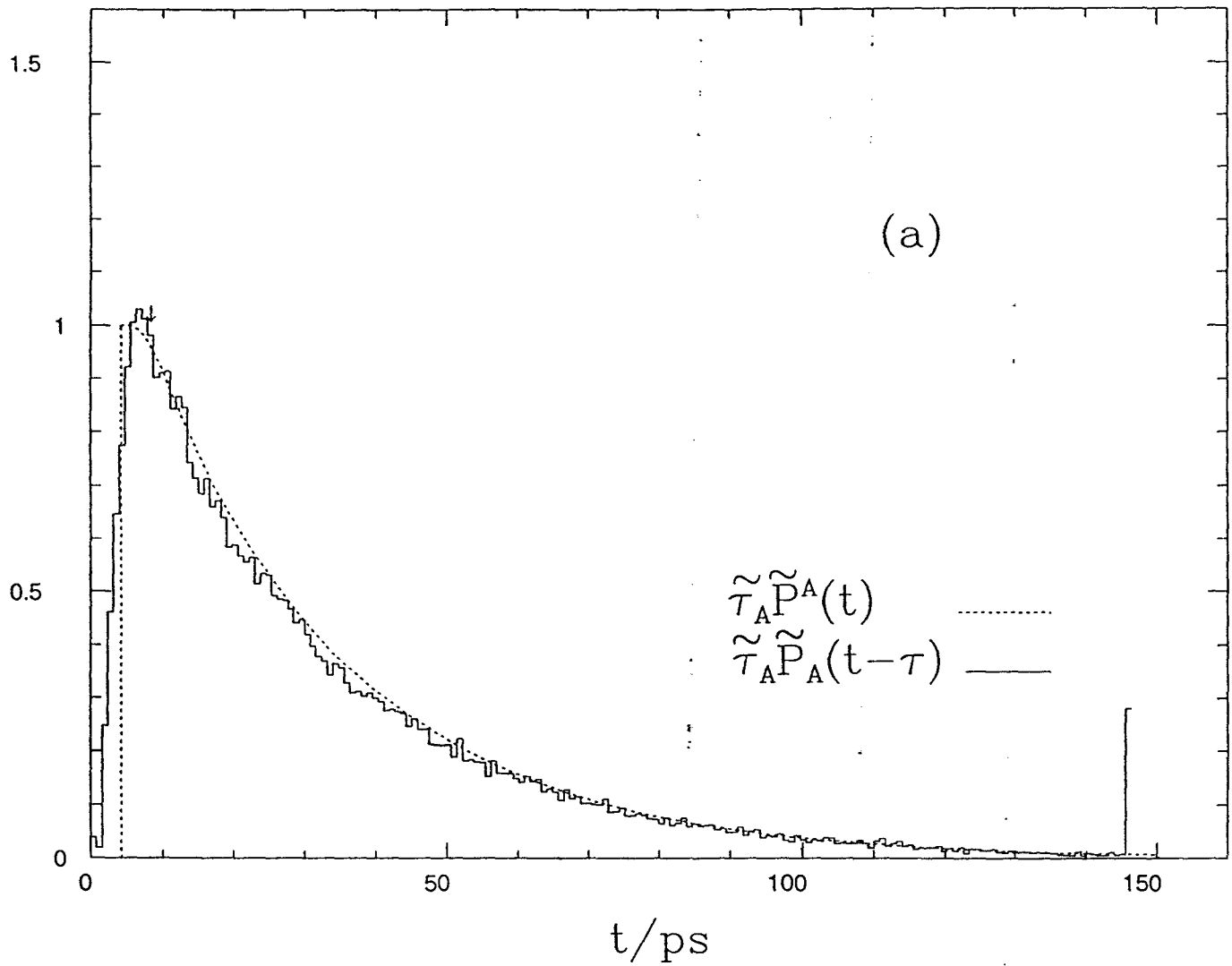

Fig. 7. As in Fig. 6 except for the incorporation of additional delay, δ [see Eq. (4.10)]. δ values employed are provided in Table 2. The arrows are placed at $t = 2\tau$. In the DLGM, this time determines the end of the gap distribution plateau.

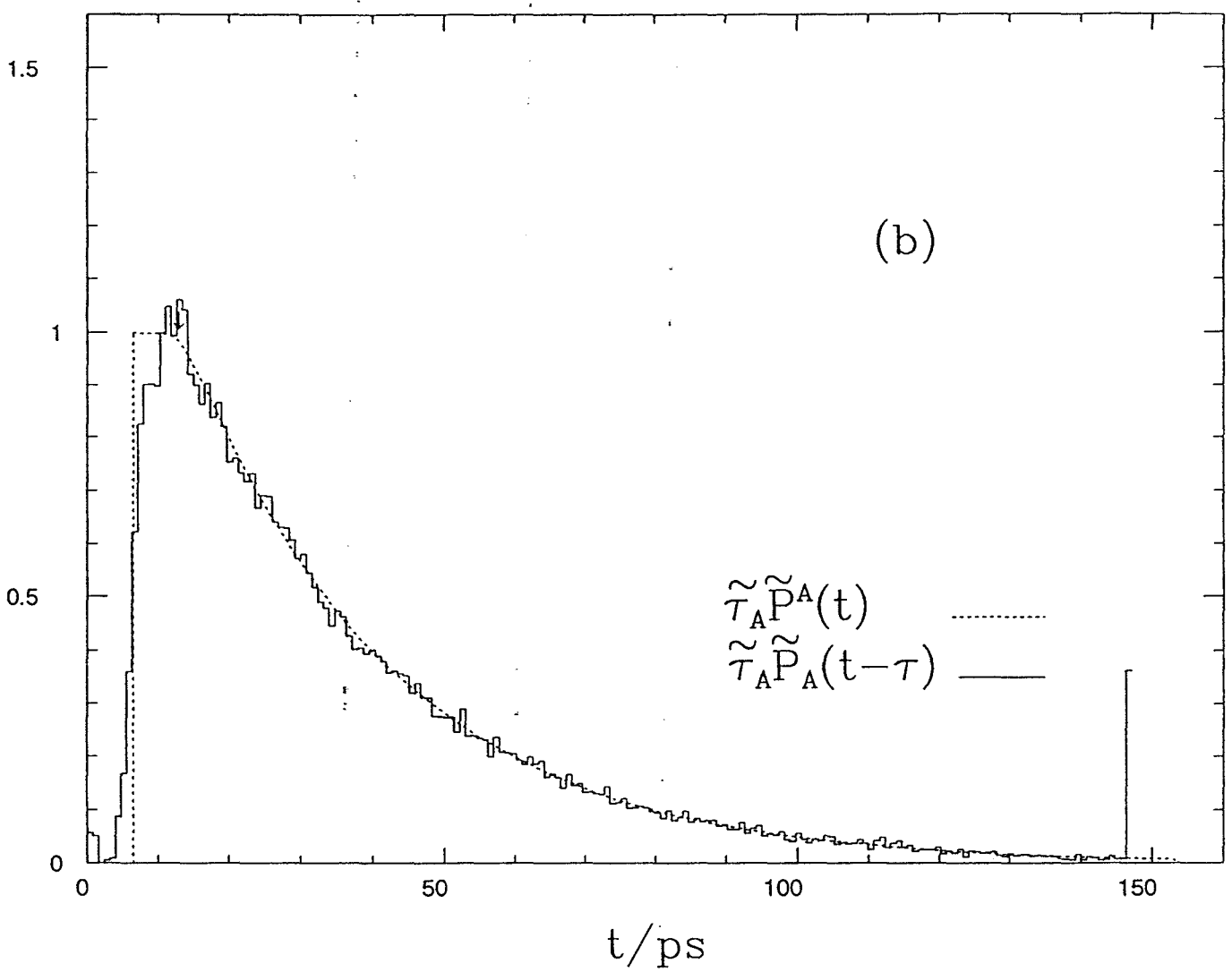

Fig. 7. As in Fig. 6 except for the incorporation of additional delay, δ [see Eq. (4.10)]. δ values employed are provided in Table 2. The arrows are placed at $t = 2\tau$. In the DLGM, this time determines the end of the gap distribution plateau.

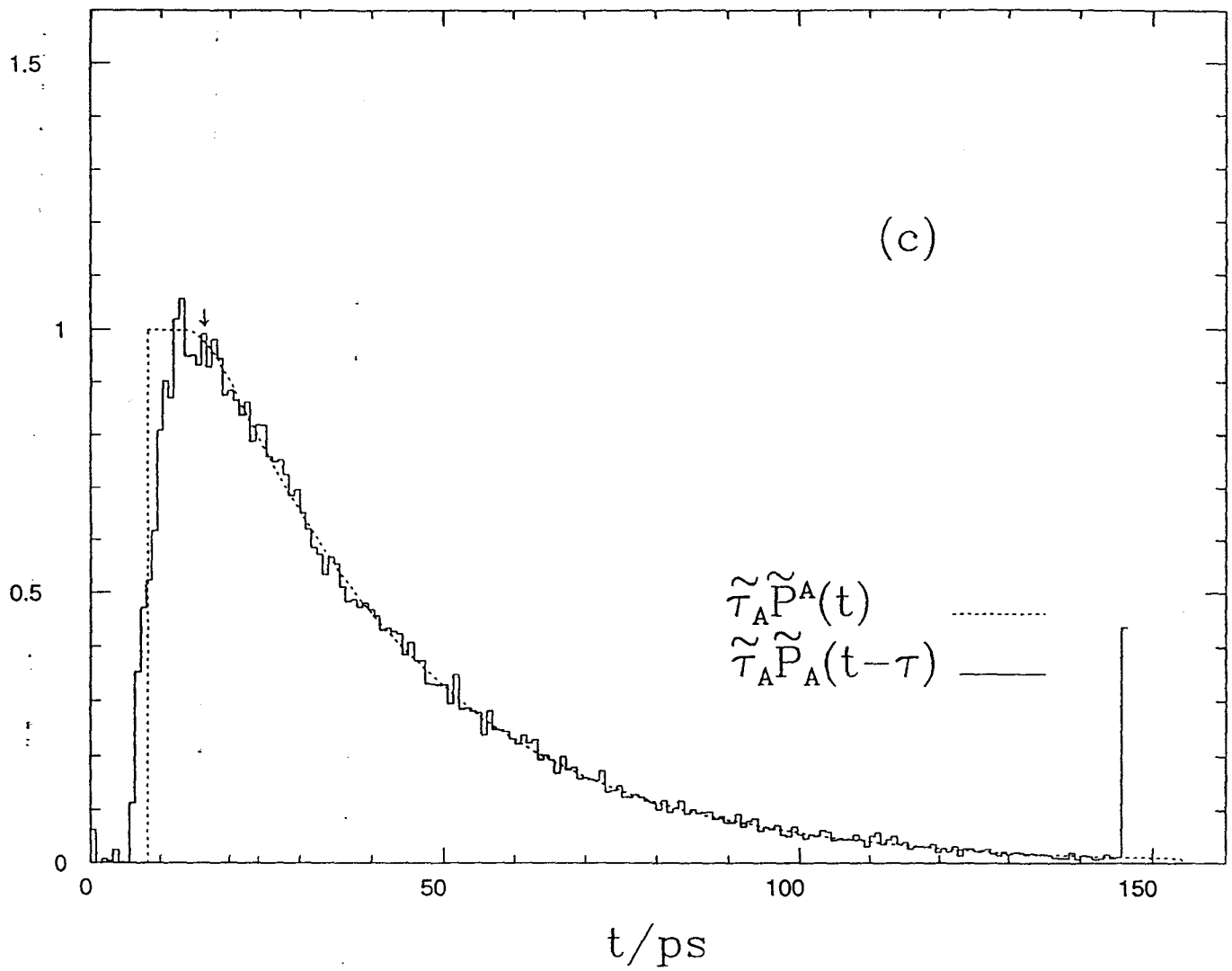

Fig. 7. As in Fig. 6 except for the incorporation of additional delay, δ [see Eq. (4.10)]. δ values employed are provided in Table 2. The arrows are placed at $t = 2\tau$. In the DLGM, this time determines the end of the gap distribution plateau.

an arrow in each panel of Fig. 7 to show where $t = 2\tau$. Since $\bar{P}^A(t)$ is plotted with a τ delay, we look for $t = 2\tau$ to correspond to the end of the plateau. The agreement is best for the larger two divergence thresholds.

(2) The adapted DLGM is characterized by an asymptotic exponential time constant, $\tilde{\tau}_{DLGM}$, which is a function of $\tilde{\tau}_A$ and τ. Specifically, $\tilde{\tau}_{DLGM}$ is the solution to the following nonlinear equation[5]:

$$\tilde{\tau}_{DLGM} = \tilde{\tau}_A \exp(-\tau/\tilde{\tau}_{DLGM}) \cdot \qquad (4.12)$$

To further test applicability of the adapted DLGM, we have fitted the observed gap and delayed lifetime distributions with exponential decays in the range $21 \text{ ps} < t < 140 \text{ ps}$. The associated time constants are provided in Table 2. DLGM gap and lifetime distributions are characterized by exponential decay according to $\tilde{\tau}_{DLGM}$ of Eq. (4.12). By comparing the observed time constants to $\tilde{\tau}_{DLGM}$, for the three D values, we conclude that $D = 10^3$ is not consistent with the DLGM. However, the DLGM is much more successful for the other D values, especially $D = 10^4$.

If there were an a priori means of predicting a divergence threshold, D, on the order of 10^4 or 10^5, then the adapted DLGM/ABM would provide a reasonably accurate minimally dynamic model of T-shaped Ar_3 inversion at $E = 150$ K. In Sec. B, directly below, we consider characteristics of the model which enable it to describe observed survival probabilities. In particular, we examine how the model is capable of describing both oscillatory (E = 150 and 160 K) and non-oscillatory (E = 144 K) population decay.

4.2. Adapted DLGM/ABM Model of Inversion

The results of Chapter 2 suggest that the T-shaped Ar_3 inversion process might be reasonably modeled by combining the adapted delayed lifetime gap model and the

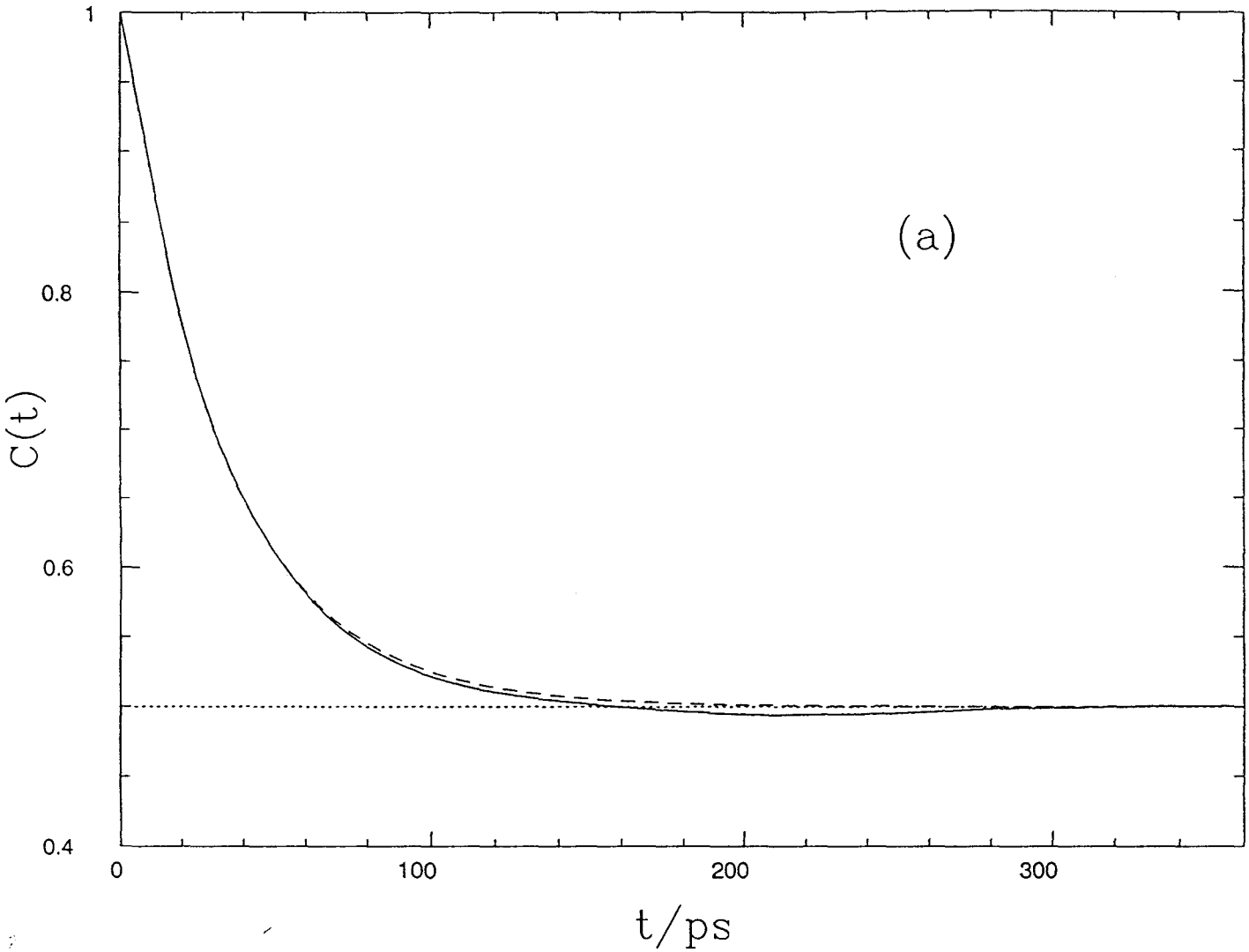

Fig. 8. As in Fig. 4 except that adapted DLGM/ABM model survival probabilities are compared with observed data. A DLGM divergence threshold of $D = 10^5$ was used for all three energies. Other parameters, τ and δ, were chosen to give the best fit to the observed data.

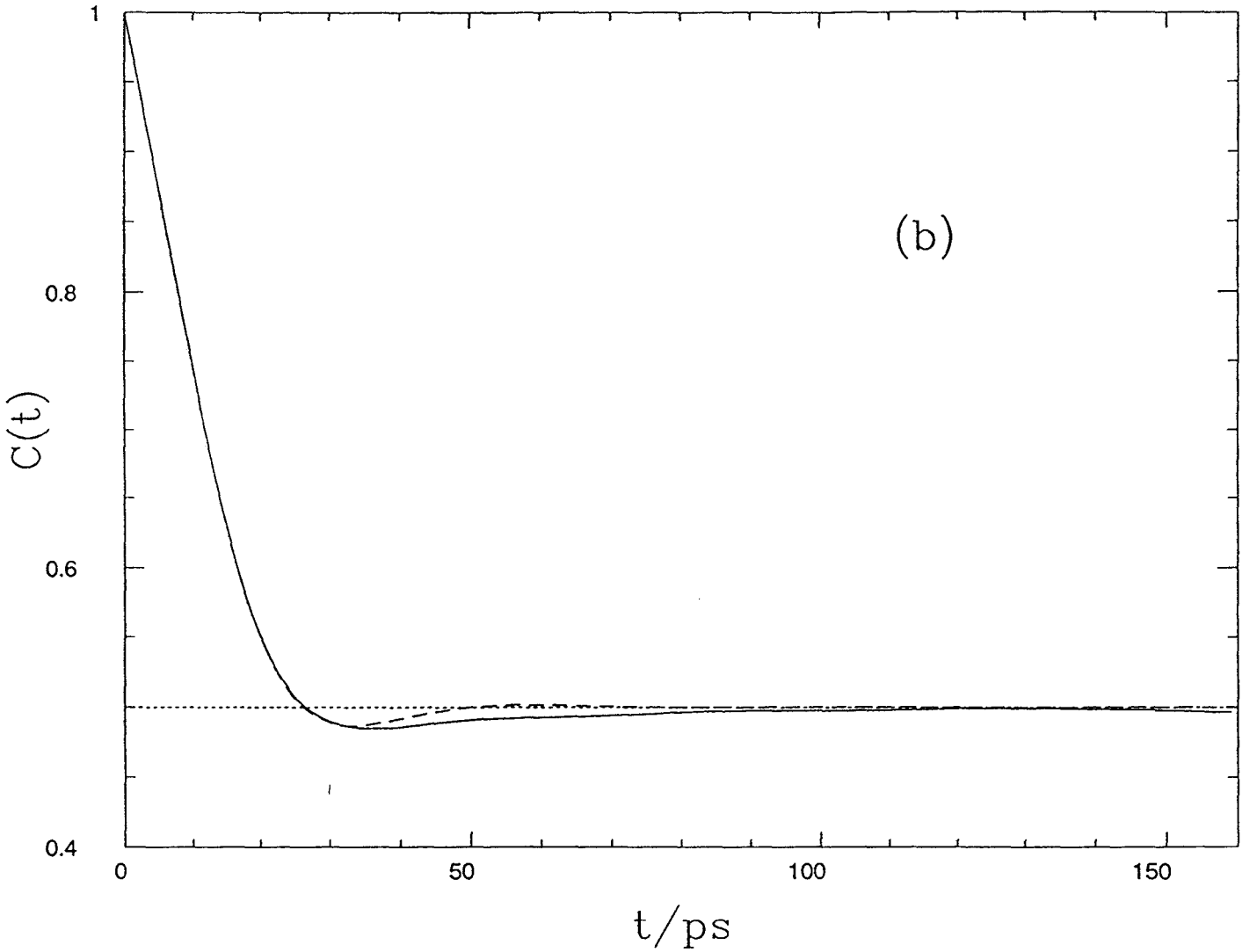

Fig. 8. As in Fig. 4 except that adapted DLGM/ABM model survival probabilities are compared with observed data. A DLGM divergence threshold of D = 10^5 was used for all three energies. Other parameters, τ and δ, were chosen to give the best fit to the observed data.

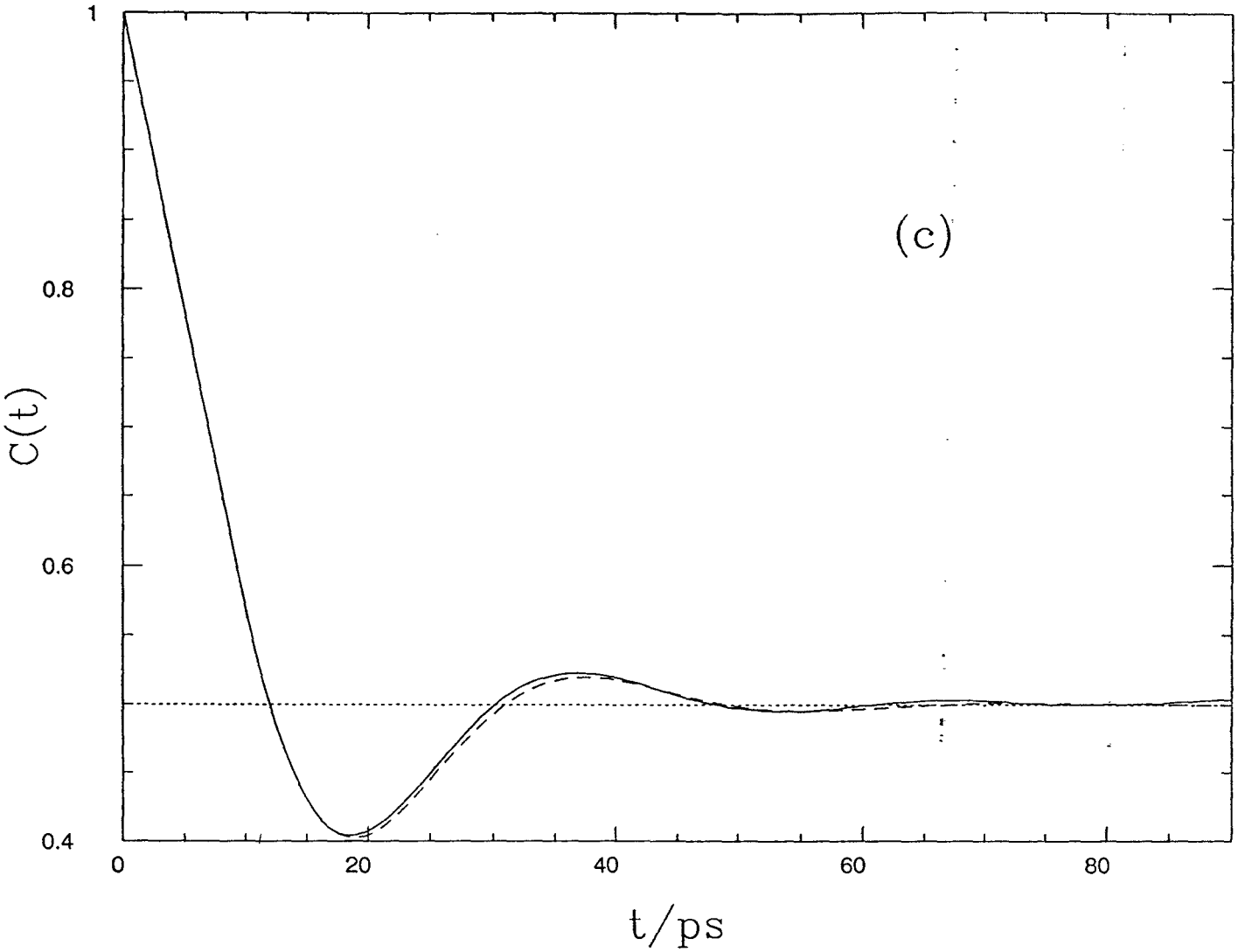

Fig. 8. As in Fig. 4 except that adapted DLGM/ABM model survival probabilities are compared with observed data. A DLGM divergence threshold of D = 10^5 was used for all three energies. Other parameters, τ and δ, were chosen to give the best fit to the observed data.

absorbing barrier method. In this section, we present survival probabilities obtained with the proposed model. Figure 8 shows model survival probabilities which correspond to the data of Fig. 4 . Clearly, the model satisfactorily reproduces characteristics of the observed survival probabilities.

It is instructive to re-examine the formulae underlying the model survival probabilities. In particular, we determine how the model is able to describe both oscillatory [Figs. 8(b) and (c)] and non-oscillatory [Fig. 8(a)] survival probabilities. First, we consider the Fourier transform of the survival probability within the ABM approximation,[5d]

$$C_{ABM}(\omega) \equiv \int_0^\infty dt \exp(-i\omega t)\, C_{ABM}(t)$$

$$= k_a\{(1 - i\omega\tau_a)[1 + P_a(\omega)] - 2P_a(\omega)\}/\{\omega^2[1 + P_a(\omega)]\} . \qquad (4.13)$$

This expression[21] follows from Eqs. (2.5a) and (2.11)

In general, the adapted DLGM is incorporated into Eq. (4.13) via substitution of the model gap distribution Fourier transform[22],

$$P_{a,DLGM}(\omega) =$$

$$f^{\alpha}P_{\alpha}(\omega) + f^{A}\exp(-i\omega\delta)/[1 + i\omega(\tau_A - \delta)\exp(i\omega\tau)]. \qquad (4.14)$$

However, we simplify the treatment below by focusing solely on the case of no direct component, i.e. $f^{\alpha} = 0$. The intent here is to provide a qualitative understanding of model oscillatory and non-oscillatory behavior. Note that it is possible to incorporate effects of a direct component into results derived below. This could be achieved in terms of formulae derived in Ref. 5d . However, such an extension requires a more detailed model of the inversion process than is considered here.

Eq. (4.14), with $f^{\alpha} = 0$, is substituted into Eq. (4.13). The resulting expression is simplified by setting τ_A to 1 . This corresponds to letting τ_A be the unit of time. In

addition, the exponentials in τ and δ are expanded and truncated to first and second order, respectively. This determines an approximation of $C_{model}(\omega)$ which neglects high frequency, or short time scale, contributions. The result is

$$C_{model}(\omega) \cong \frac{-i}{2\omega} + \frac{1}{2\alpha}\frac{1 + \beta^2 - 2\alpha + i\omega\alpha}{(\beta/\alpha + i\omega)^2 - (\beta^2/\alpha - 4)/\alpha}, \qquad (4.15)$$

where $\alpha = 2(1 - \delta)\tau + \delta^2$ and $\beta = 1 - 2\delta$.

The first term of Eq. (4.15) is a pole at $\omega = 0$. It corresponds to the equilibrium population of 1/2. Specifically, it determines the long time limit, $C_{model}(\infty) = 1/2$. The denominator of the second term is easily factored to reveal two other poles of $C_{model}(\omega)$. The Fourier inversion theorem and the Cauchy integral formula relate these poles to exponential decay rates (a pole at $\omega = \omega_0$ corresponds to a decay rate of $-i\omega_0$). The decay rates are purely real as long as $\beta^2/\alpha - 4$ is positive. This is the regime of E = 144 K.

The survival probability of Eq. (4.15) is analogous to the amplitude of a damped harmonic oscillator[23]. In this analogy, $2/\sqrt{\alpha}$ and $2\beta/\alpha$ are identified with a harmonic oscillator frequency and a friction coefficient, respectively. Just like the damped harmonic oscillator, our model survival probability has "overdamped" and "underdamped" conditions. The latter are determined by the sign of $\beta^2 - 4\alpha$.

The overdamped conditions of $\beta^2 > 4\alpha$ include the chemical kinetics limit, where δ and $\tau \to 0$ (and consequently $\alpha \to 0$ and $\beta \to 1$). Specifically, in this case we have

$$C_{model}(\omega) \sim \frac{-i}{2\omega} + \frac{1}{2}\frac{1}{(2 + i\omega)}. \qquad (4.16)$$

Here, the transient population decays with rate 2 (or $2k_a$, if the frequency units of $k_a = k_A = 1/\tau_A$ are made explicit), and the weight of this $\exp(-2k_a t)$ decay is 1/2. This is just the kinetics result for simple isomerization.

If $\beta^2 < 4\alpha$, then the decay rates have imaginary parts. An imaginary component to a decay rate corresponds to an oscillation frequency. This is the case of an "underdamped" harmonic oscillator. In particular, this case corresponds to the observed survival probabilities at E = 150 and 160 K. The transition to underdamped oscillations occurs when $\beta^2 = 4\alpha$. This determines a curve in (δ,τ) space, depicted in Fig. 9. This curve separates the overdamped region, of small δ and τ, from the underdamped region (the regions are labeled in the figure). Note that if either δ or τ is sufficiently large, then underdamping and the associated oscillatory survival probability behavior result. However, sufficiently large δ and τ are likely to occur together as a result of τ_A being insufficiently large to produce overdamping. Recall that δ and τ, as they appear in the above formulae, are actually ratios with respect to τ_A. Thus, the model of Eq. (4.15) illustrates the principle, described above, which associates nonstatisticality with a nonseparation of time scales. Specifically, statisticality results under mixing conditions if the reaction process time scale, τ_A, is sufficiently long compared with internal relaxation time scales, δ and τ. When the time scale separation does not occur, nonstatisticality appears and can take the form of an oscillatory survival probability.

In principle, one could determine a lowest energy for which the T-shaped Ar_3 inversion process would first begin to exhibit survival probability oscillations. However, a quantitative analysis requires inclusion of direct component effects into the model presented above. It also requires a firmer basis for choosing the relevant model parameters, δ, τ, and D. At present, we are content with a qualitative understanding of the characteristics of nonstatisticality. Further investigations will be concerned with more quantitative approaches, and with more complex intramolecular dynamical processes.

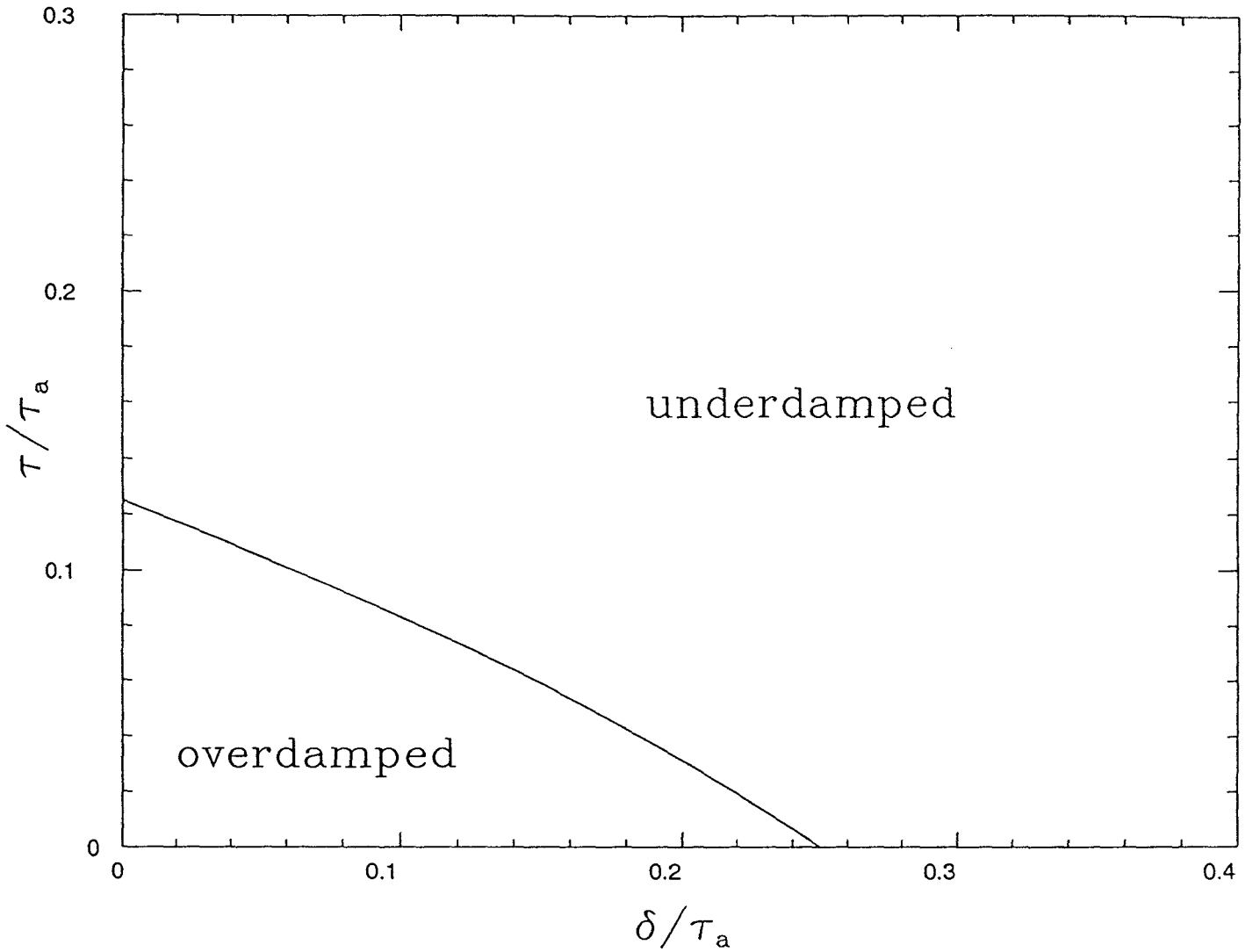

Fig. 9. Overdamped and underdamped regions in delay time, τ and δ, parameter space. The boundary between these regions is depicted as a solid curve. It is determined by $\beta^2 = 4\alpha$. Note that the axis labels make the time unit of τ_a explicit.

Chapter 5

Conclusion

Chapter 5

Conclusion

Nonstatisticality of T-shaped Ar_3 inversion has been established via trajectory computations. It is most pronounced at higher energies where the inversion time scale is small compared with internal relaxation times. In particular, higher energies are associated with oscillatory survival probabilities. Lower energies, approaching the inversion threshold, have larger inversion time scales and nonoscillatory, near statistical survival probabilities.

The observed data have been modeled using a combination of the absorbing barrier method and an adaptation of the delayed lifetime gap model. The model survival probabilities seem to capture the essential features of the observed survival probabilities, specifically the overshoot of the asymptotic population of 1/2 and oscillatory behaviour at energy, E = 160 K and overshoot but no subsequent oscillations at energy, E = 150 K. At energy, E = 144 K , nearly statistical behaviour is reproduced.

The adapted model incorporates an additional delay (i.e. in addition to the DLGM delay, τ) to account for slow exponential divergence in the neck region of the T-shaped Ar_3 potential well. Analysis of the model employed reveals a damped harmonic oscillator analogy. Near-threshold energies correspond to the "overdamped" regime of the harmonic oscillator, while higher energies are in the "underdamped" regime and naturally exhibit oscillatory survival probabilities.

The model employed above required choices for DLGM parameters, D and τ. D is the divergence threshold which defines the strong collision component, and τ is an internal relaxation time. These parameters were chosen above to give best agreement between shifted gap and delayed lifetime distributions. If these parameters were predictable, then the model could have been implemented in an a priori, minimally dynamic fashion. In particular, explicit computation of trajectories only up to a divergence of just beyond D would provide sufficient information to implement the model. (We must go beyond D , in order to estimate the height of the gap distribution plateau.) However, while some guides to choosing D and τ do exist.[5] they are not sufficiently general, and the goal of a comprehensive a priori statistical theory of unimolecular reactions has not been reached. Nevertheless, the model presented here provides insight into a source of nonstatistical population decay in isomerization reactions, since inversion of T-shaped Ar_3 is a prototype for simple isomerization. In addition, we have investigated ideas that could lead to a quantitative treatment of the "transition to nonstatisticality" that occurs as energy is increased.

Future investigations will be concerned with the development of a comprehensive statistical theory of unimolecular reactions, and with the exploration of more complex unimolecular processes and any associated nonstatistical phenomena.

REFERENCES

References and Footnotes:

1. (a) R. A. Marcus and O. K. Rice, J. Phys. Coll. Chem. 55, 894 (1951) ; S. Gladstone, K. J. Laidler, and H. Eyring, *The Theory of Rate Proces* (McGraw-Hill, New York, 1941); P. Pechukas, in *Dynamics of Molecular Collisions*, Part B, edited by W. H. Miller (Plenum, New York, 1976) ; (b) For a recent review, see B. J. Berne, M. Borkevec, and J. E. Straub, J. Phys. Chem 92, 3711 (1988).
2. W.L. Hase, in *Dynamics of Molecular Collisions, Part B*, ed. W.H. Miller, (Plenum Press, New York, 1976) for an introduction to statistical theories of unimolecular reactions; D. M. Wardlaw and R. A. Marcus, Chem. Phys. Lett. 110, 230 (1984); D. G. Trulhar, W. L. Hase, and J. T. Hynes, J. Phys. Chem. 87, 2664 (1983).
3. N. DeLeon B. J. Berne, J. Chem. Phys. 75, 3495 (1981); R. J. Wolf W. L. Hase, *ibid.* 72, 316 (1980).
4. M. J. Davis, J. Chem. Phys. 83, 1016 (1985); M. J. Davis and S. K. Gray, *ibid.* 84, 5389 (1986); S. K. Gray, S. A. Rice, and M. J. Davis, J. Phys. Chem. 90, 3470 (1986); S. K. Gray and S. A. Rice, J. Chem. Phys. 86, 2020 (1987).
5. a) R.S. Dumont and P. BcGraw, J. Phys. Chem. 90, 3509 (1986);
   b) R.S. Dumont and P. Brumer, submitted to Chem. Phys. Lett.;
   c) R.S. Dumont, J. Chem. Phys. 91, 4679 (1989);
   d) *ibid.* 6839 (1989).

6. I. Hamilton and P. Brumer, J. Chem. Phys. 82, (1985). For applications to bimolecular reactions, see J. W. Duff and P. Brumer, J. Chem. Phys. 71, 3895 (1979), and references therein.

7. For example, bottleneck analyses are currently based on surface of section techniques. The quantitative components of this methodology are so far restricted to two degree of freedom systems. Divergence, on the other hand, can be calculated for any conservative, deterministic dynamical system.

8. Zero angular momentum Ar_3 , in three dimensions, has been shown to possess dynamical characteristics typical of chaos. See T.L. Beck, D.M. Leitner and R.S. Berry, J. Chem. Phys. 89, 1681 (1988).

9. The nonstatisticality of chaotic T-shaped Ar_3 contrasts recent claims of a strict connection between chaos and statistical unimolecular decay. See W. Bauer and G.F. Bertsch, Phys. Rev. Lett. 65, 2213 (1990).

10. J.E. Straub and B.J. Berne, J. Chem. Phys. 83, 1138 (1985); and J.E. Straub, D.A. Hsu, and B.J. Berne, J. Phys. Chem. 89, 5188 (1985).

11. R.S. Dumont, Ph.D. Dissertation University of Toronto (1987).

12. R.A. Aziz and M.J. Slaman, Mol. Phys. 58, 679 (1986).

13. a) Energy is measured in units of K , via scaling by Boltzmann's constant.
b) The atomic unit of time consistent with energy units of K is $\hbar$/K ;
1 $\hbar$/K = 7.6383 ps . However, times reported here, are given in ps .
c) Distance is measured in Bohr; 1 Bohr = 0.52918×10^{-8} cm .
d) The usual atomic unit of mass, the "electron", is modified by the energy conversion factor of Hartrees to Kelvin; 1 electron Hartree/K = 173.17 amu .

14. If the energy hypersurface $H(\Gamma) = E$ is metrically decomposable into regular and irregular regions, then any given trajectory crossing the barrier will not be able

to visit some measurable regions of phase space. The motion will then be nonergodic.

15. V. I. Arnold and A. Avez, *Ergodic Problems of Classical Mechanics*(Benjamin, New York, 1968).

16. R.S. Dumont, J. Comp. Chem. **12**, 391 (1991).

17. D. Chandler, J. Chem. Phys. **68**, 2959 (1978). See also Ref. 5b .

18. Two types of islands occur in phase space, Trapping Islands (T) and Crossing Islands (C). Motion on T corresponds to librations in one or another well with no crossing of the barrier while, motion on C corresponds to frequent crossing of the barrier with no trapping. Presence of T reduces volume of phase space available for the propagation of the trajectories. which shortens the mean gap time,τ (= phase space volume/flux across transition state). Presence of Crossing Islands also reduces phase space volume but flux across the transition state is also reduced and the net effect is to enhance the mean gap time.

19. I. C. Percival, Proc. R. Soc. Lond. A 413, 131 (1987).

20. See Ref. 5d and N.G. van Kampen, *Stochastic Processes in Physics and Chemistry* (North-Holland, Amsterdam, 1981).

21. Integrating by parts of Fourier Transform of both sides of Eq. (2.5a) and using Eq. (2.4a), we get: $k(\omega) = 1 - i\omega\, C(\omega)$. Similar treatment on Eq. (2.11) gives: $F(\omega) = 1 - i\omega\, \tau_a\, k(\omega)$. Substituting for $k(\omega)$ from above , Eq. (3.6a) for $F(\omega)$ and rearranging, we get the desired expression for $C(\omega)$.

22. This is just the DLGM gap distribution Fourier transform [see Eq. (4.7)], except for the additional $\exp(-i\omega\delta)$ factor and the shift of τ_A by δ . The latter two modifications constitute the Fourier representation of the shift by δ transformation.

23. The amplitude of a damped harmonic oscillator satisfies the following differential equation,

$$\ddot{x} + \omega_0^2 x + \gamma \dot{x} = 0 \ .$$

Its solution has the Fourier representation,

$$x(\omega) = \int_0^\infty dt \exp(-i\omega t)\, x(t)$$

$$= \frac{\dot{x}(0) + (i\omega + \gamma)x(0)}{\omega_0^2 + i\gamma\omega - \omega^2}$$

$$= \frac{\dot{x}(0) + (i\omega + \gamma)x(0)}{(\omega_+ + i\omega)(\omega_- + i\omega)}$$

where $\omega_\pm = \gamma/2 \pm i(\omega_0^2 - \gamma^2/4)^{1/2}$ are interpretable as decay rates. When $\omega_0^2 - \gamma^2/4 < 0$, the decay rates are real and the oscillator is "overdamped". If $\omega_0^2 - \gamma^2/4 > 0$, the decay rates have imaginary parts which correspond to oscillation frequencies. In this case, the oscillator is said to be "underdamped". Comparison with the model survival probability of Eq. (4.15) yields the identification of model parameters, $2\beta/\alpha$ and $2/\sqrt{\alpha}$, with damped harmonic oscillator parameters, γ and ω_0, respectively.

APPENDIX

Appendix

Monte Carlo Sampling According to Microcanonical Flux Density

Gap distributions and flux-flux correlations computed for this article can be viewed as averages of delta function phase space densities over microcanonical flux density weighted transition states. For example, the first term of the flux-flux correlation, in Eq. (2.14), is expressible as

$$\begin{aligned} < j^a_t j^b >/< j^a > &= < j^a j^b_{-t} >/< j^a > \\ &= < f >_{\rho^a} \\ &\equiv \int dq\, dp\, \rho^a(q,p)\, f(q,p;t) \end{aligned} \tag{A1a}$$

where

$$\rho^a(q,p) = j^a(q,p)/< j^a > , \tag{A1b}$$

is the normalized microcanonical flux density on S^a [see Eq. (2.7) for j^a], while

$$f(q,p;t) = \sum_{j=1}^{\infty} \delta[t - t^b_{cross,j}(q,p)] \tag{A1c}$$

is a t dependent delta function phase space density. $t^b_{cross,j}(q,p)$ is the j th time at which the trajectory initialized at (q,p) crosses S^b. Note that, in practice, the delta functions of f are replaced by step functions, and the flux-flux correlation is thereby computed as a histogram. The other contributions to flux-flux correlation in Eq. (2.14) are similarly expressed. In the case of a gap distribution, the function f consists of only the first term of Eq. (A1c).

From Eq. (A1), we see that the flux-flux correlation is computed from an ensemble of trajectories initialized on S^a, weighted according to the microcanonical flux density. This Appendix describes the Monte Carlo method used to carry out the necessary sampling of the initial conditions on S^a.

We treat the case of an n degree of freedom system, making use of simplifying features of the Hamiltonian of Eq. (2.1) and the transition state of Eq. (2.8).

$$H(q,p) = T(p) + V(q)$$
$$= \sum_{i=1}^{n} \frac{p_i^2}{2\, m_i} + V(q) \ . \qquad \text{(A2)}$$

The transition state, S^a, is defined by $q_1 = 0$, as in Eq. (2.7). The associated flux density is given by

$$j^a(q,p) = \frac{p_1}{m_1} \theta(p_1)\, \delta(q_1)\, \delta[E - H(q,p)] \ . \qquad \text{(A3)}$$

The support of j^a is restricted to $q = q^* \equiv (0,q')$, the transition state projected configuration; $q' = (q_2,\ldots,q_n)$ gives configuration coordinates on S^a, and $\theta(p_1) = 1$ or 0 if $p_1 >$ or < 0 respectively.

With the above Hamiltonian and transition state, the integration in Eq. (A1a) over q_1 is performed explicitly and the p integration is subject to a special treatment. Specifically,

$$< f > =$$
$$= \int_S dq' \, [\varphi_{\varepsilon(q^*)}/\Phi] \int_{\mathbb{R}^n} dp \, \rho_{\varepsilon(q^*)}(p)\, f(q^*,p;t) \ , \qquad \text{(A4a)}$$

where

$$\rho_\varepsilon(p) = \frac{p_1}{m_1}\,\theta(p_1)\,\delta[\varepsilon - T(p)]/\varphi_\varepsilon \ , \tag{A4b}$$

$$\varphi_\varepsilon(q) = \int_0^\infty dp_1 \frac{p_1}{m_1}\int_{\mathbb{R}^{n-1}} dp_2 \ldots dp_n\ \delta[\varepsilon - T(p)]$$

$$= \begin{cases} \dfrac{\pi^{(n-1)/2}}{\Gamma[(n+1)/2)]}(2\varepsilon)^{(n-1)/2}\displaystyle\prod_{i=2}^{n} m_i^{1/2} & , \varepsilon > 0 \\ & , \varepsilon \le 0 \end{cases} , \tag{A4c}$$

$$\varepsilon(q) = E - V(q) \tag{A4d}$$

while

$$\Phi = \langle j^a \rangle = \int_S dq'\ \varphi_{\varepsilon(q^*)} \tag{A4e}$$

is the total flux through S^a. S is the projection of S^a onto $\mathbf{q}'$ space. Equation (A4a) expresses $\langle f \rangle$ in terms of average values in the $\mathbf{q}'$ and p spaces, S and $\mathbb{R}^n$ respectively. Specifically,

$$\langle f \rangle = \langle \langle f^b \rangle_{\rho_\varepsilon} \rangle_\varphi \ ; \tag{A5}$$

i.e., $\langle f \rangle$ is expressed as a $\mathbf{q}'$ space average, with respect to density $\varphi(q') \equiv \varphi_{\varepsilon(q^*)}/\Phi$, of a p space average, with respect to density $\rho_{\varepsilon(q^*)}$.

Although the average over momentum space involves a delta function density, it is possible to construct a simple Monte Carlo scheme for sampling momentum because of the quadratic momentum dependence of the kinetic energy. The scheme starts by sampling the reaction coordinate "mode kinetic energy", $\varepsilon_1 = p_1^2/2m_1$, according to its "marginal distribution",

$$\kappa_1(\varepsilon_1) \equiv \int_0^\infty dp_1 \frac{p_1}{m_1}\,\delta\left[\varepsilon_1 - \frac{p_1^2}{2m_1}\right]\int_{\mathbb{R}^{n-1}} dp_2 \ldots dp_n\ \delta[\varepsilon - T(p)]/\Phi$$

$$= (n-1)(1 - \varepsilon_1/\varepsilon)^{(n-3)/2}/(2\varepsilon)\ \theta(\varepsilon - \varepsilon_1) \ , \tag{A6}$$

where $\varepsilon = \varepsilon(q^*)$.

The cumulative probability distribution $\zeta(\varepsilon_1)$, is given by,

$$\zeta(\varepsilon_1) = \int_0^{\varepsilon_1} d\varepsilon_1' \, \kappa_1(\varepsilon_1')$$
$$= 1 - (1 - \varepsilon_1/\varepsilon)^{(n-1)/2} \qquad \text{(A7)}$$

Now a random number, ζ , uniformly distributed on (0,1) is choosen and if ζ^{-1} denotes the inverse cumulative probability, then ε_1 is given by

$$\zeta = \zeta(\varepsilon_1)$$

or,

$$\varepsilon_1 = \zeta^{-1}(\zeta)$$
$$= \varepsilon(q^*) \, [1 - (1 - \zeta)^{2/(n-1)}] \; . \qquad \text{(A8)}$$

The remaining mode kinetic energies, $\varepsilon_i = p_i^2/2m_i$ (i = 2,...,n), are then sampled identically and independently, except for the constraint that their sum equals the remaining kinetic energy, $\varepsilon(q^*) - \varepsilon_1$. This sampling is achieved by generating n - 2 independent random numbers uniformly distributed in (0 , 1), $\{\zeta_i\}_{i=2}^{n-1}$. After sorting the random numbers in ascending order (i.e. relabeling them so that $\zeta_{i+1} > \zeta_i$), the desired sampled mode energies are obtained from

$$\varepsilon_i = [\varepsilon(q^*) - \varepsilon_1] \, (\zeta_i - \zeta_{i-1}) \; , \; i = 2,...,n \; , \qquad \text{(A9a)}$$

with the convention, $\zeta_1 = 0$ and $\zeta_n = 1$. Associated momenta are determined at random by

$$p_i = \pm \, (2 \, m_i \varepsilon_i)^{1/2} \; , \qquad \text{(A9b)}$$

with + and - equally likely.

In the case of T-shaped Ar_3 , the **q'** sampling is trivial. S is a simple one dimensional interval. However, in cases where n > 2 , S can be complicated and difficult to sample according to $\varphi(\mathbf{q}')$. In such more general cases, the **q'** space average value is best evaluated with a **q'** space Metropolis random walk.